Al2O3-ZnO atomic layer deposited nanolaminates for improving mechanical and corrosion properties of sputtered CrN coatings

Elias Kaady, Akram Alhussein, Mikhael Bechelany, Roland Habchi

▶ **To cite this version:**

Elias Kaady, Akram Alhussein, Mikhael Bechelany, Roland Habchi. Al2O3-ZnO atomic layer deposited nanolaminates for improving mechanical and corrosion properties of sputtered CrN coatings. Thin Solid Films, 2022, 759, pp.139476. 10.1016/j.tsf.2022.139476 . hal-03844971

HAL Id: hal-03844971

https://hal.umontpellier.fr/hal-03844971v1

Submitted on 18 Nov 2022

HAL is a multi-disciplinary open access archive for the deposit and dissemination of scientific research documents, whether they are published or not. The documents may come from teaching and research institutions in France or abroad, or from public or private research centers.

L'archive ouverte pluridisciplinaire **HAL**, est destinée au dépôt et à la diffusion de documents scientifiques de niveau recherche, publiés ou non, émanant des établissements d'enseignement et de recherche français ou étrangers, des laboratoires publics ou privés.

Al2O3-ZnO atomic layer deposited nanolaminates for improving mechanical and corrosion properties of sputtered CrN coatings

Elias KAADY [1, 2,*], Akram ALHUSSEIN [1], Mikhael BECHELANY [3] and Roland HABCHI [2,*]

[1] *UR LASMIS, Université de Technologie de Troyes, Pôle Technologique Sud Champagne, 52800 Nogent, France.*

[2] *EC2M, Faculty of Sciences, Campus Pierre Gemayel, Lebanese University, Fanar, 90656, Lebanon.*

[3] *Institut Européen des Membranes, IEM, UMR 5635, Univ. Montpellier, ENSCM, CNRS, Montpellier, France.*

** Corresponding authors: Elias KAADY, elias.kaady@utt.fr ; Roland HABCHI, rhabchi@ul.edu.lb .*

Abstract

AISI 316L Stainless Steel, widely used as structural material in marine applications, is subject to localized pitting corrosion in chloride ions rich environment. The main aim of the present work is the development of duplex coatings deposited alternately by both PVD and ALD techniques, the evaluation of their combination effect and the comparison between different materials and architectures. Three different architectures PVD/ALD, ALD/PVD and PVD/ALD/PVD were elaborated in this study. Atomic layer deposited Al_2O_3, ZnO and Al_2O_3-ZnO nanolaminates thin films were inserted as sealing, top and inter layers within CrN sputtered films. The texture modification, morphology, preferred orientation growth, mechanical properties, wettability and corrosion resistance were investigated. The nanoindentation measurements confirmed the increase in order of two GPa for the hardness of the studied coatings. Electrochemical properties and corrosion behavior of these films were studied within immersion in 3.5 wt% NaCl solution. The S/PVD/ALD/PVD architecture is the most efficient architecture to provide an improvement in corrosion resistance. The CrN/$[Al_2O_3$-ZnO$]_n$/CrN coating presents the best corrosion protection performance with the lowest I_{corr} ~ 7.9 x 10^{-10} A/cm^2 , lower two order of magnitude than I_{corr} of the substrate ~1.5 x 10^{-8} A/cm^2. The combinatorial approaches used in our study present a great potential for advanced coatings with

specific compositions that can be effectively used for different applications, especially in corrosive environments.

Keywords: *Chromium nitride (CrN); Magnetron sputtering (PVD); Atomic layer deposition (ALD); Zinc oxide (ZnO); Corrosion; Mechanical properties.*

Highlights

- Mechanical and electrochemical properties of hybrid duplex coatings elaborated by magnetron sputtering and atomic layer deposition are studied.
- ALD layer insertion, whatever the architecture is, smooths the surface.
- An increase in order of two GPa of coatings hardness is due to refinement of grains of the CrN.
- The S/PVD/ALD/PVD coatings exhibit a change in the wettability compared to CrN and is the most efficient architecture to provide an improvement in corrosion resistance.
- The CrN/$[Al_2O_3$-ZnO$]_n$/CrN coating presents the best corrosion protection performance with the lowest $I_{corr} \sim 7.9 \times 10^{-10}$ A/cm^2 lower two order of magnitude than I_{corr} of the substrate.

Graphical Abstract

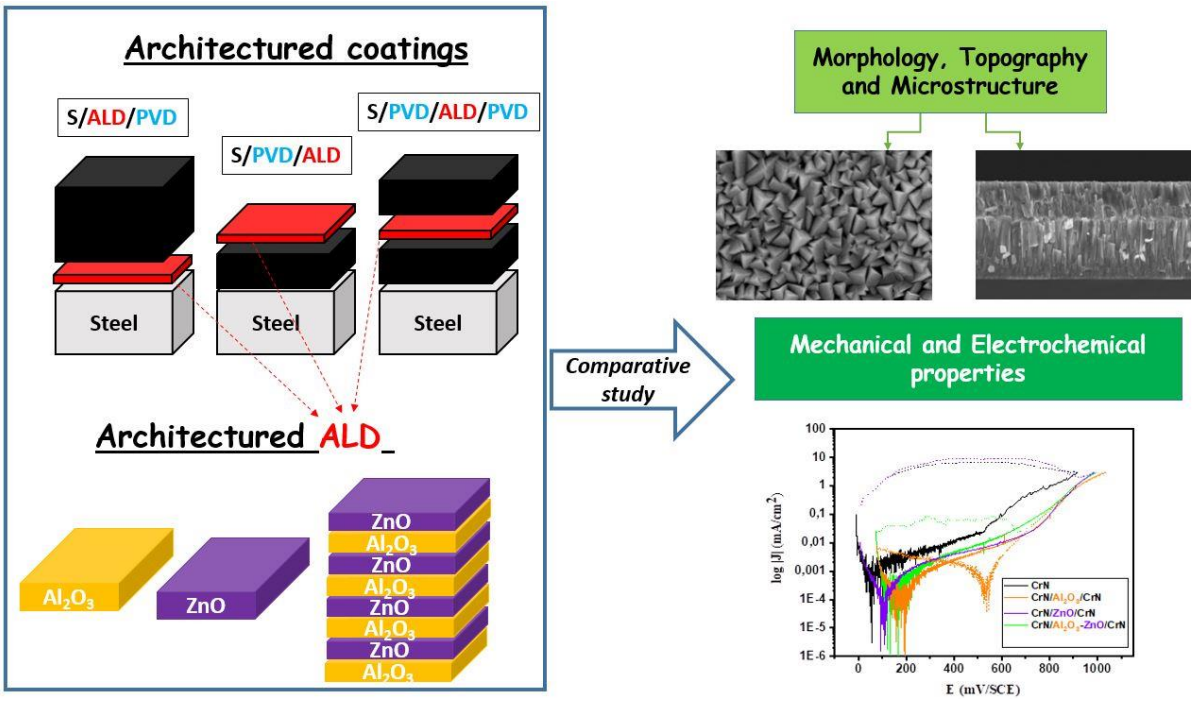
Architectured coatings
S/ALD/PVD
S/PVD/ALD
S/PVD/ALD/PVD
Steel
Steel
Steel
Architectured ALD
Al2O3
ZnO
ZnO
Al2O3
ZnO
Al2O3
ZnO
Al2O3
ZnO
Al2O3
Comparative study
Morphology, Topography and Microstructure
Mechanical and Electrochemical properties
log |J| (mA/cm²)
E (mV/SCE)
CrN
CrN/Al2O3/CrN
CrN/ZnO/CrN
CrN/Al2O3-ZnO/CrN

1. INTRODUCTION

AISI 316L Stainless Steel is widely used as structural material in marine, biomedical [1] and industrial applications due to its specific strength, fracture toughness and excellent corrosion resistance. However, AISI 316L is subject to localized pitting corrosion in chloride ions rich environment due to the breakdown of the chromium oxide thin passive layer enriched surface [2]. Facing this problem, coatings are used to protect steels [3] from chloride ions diffusion, to control their interaction with surrounding atmosphere and to extend their lifetime and corrosion durability. Hence, it is imperative to develop hard coatings with high corrosion resistance performance in marine related applications.

Even if Chemical Vapor Deposited CVD coatings are still dominating the industry, a particular importance is rising for the development of physical vapor deposition PVD coatings to benefit from their advantages. Indeed, ecological needs have favored the replacement of CVD coatings because PVD technologies do not release toxic chemicals into the environment. Likewise, PVD methods use a lower processing temperature compared to CVD [4]. High hardness, low friction coefficients and high wear resistance constitute an assembly of characteristics that had increased the use of PVD coatings to improve performance and service lifetime of tools. However, PVD coatings generally exhibit many inherent defects; including columnar structures, pores, cracks and discontinuities [5]. These defects generally generate cracks affecting significantly the resistance to corrosion and the toughness of PVD coatings.

Chromium nitride CrN coatings deposited by PVD have a great potential in the enhancement of electrochemical and mechanical surface properties because they show high hardness and good wear-corrosion resistance [6–8]. These coatings are used to protect materials in mechanical assemblies for long-term service in marine applications [9]. However, the PVD process produce columnar grown CrN with many imperfections that decrease their performance. The porosity between columnar microstructures and channels generated after imperfections delamination (like nodular delamination), leads to the diffusion of chloride ions that can penetrates into the steel and easily attack it. A serious pitting corrosion is then triggered due to direct routes and paths created in the PVD grown CrN.

Many efforts were devoted to improve CrN performance but they were limited due to some drawbacks such as:

1) alloying CrN with ternary elements (Si, B…), in order to obtain nanocomposite, was limited because the physical and chemical properties depend on the local composition and the anisotropic microstructure [10], [11], even if these nanocomposites demonstrate improved mechanical properties.

2) Multilayer or interlayer CrN/PVD layers were not successful due to shadow effect [12] or due to the decrease in mechanical properties particularly in CrN/metal layers.

3) Other strategies [8] were used to eliminate microstructural defects during the deposition process or to densify the structure by varying the deposition parameters such as bias voltage, pressure and deposition temperature. Several comparative studies [13–15] were performed on CrN elaborated by different PVD techniques such as arc evaporation and various magnetron sputtering techniques, including conventional direct current DC, radio frequency RF, pulsed DC and high power pulsed magnetron sputtering HiPIMS. After these studies one can conclude that the CrN_x microstructure and properties were directly related to the intrinsic characteristics of the generated plasma. Thus, magnetron sputtering has several advantages over conventional sputtering and other PVD techniques: the plasma created in the chamber is confined and closer to the surface of the cathode and gas ionization is realized at a lower pressure. This will significantly increase the deposition yield, improve the purity of the coatings, increase the deposition rates to several µm / min and increase the ionization efficiency. Indeed, deposits quality is also improved because incident particles undergo less collision during their trajectory between the target and the substrate. In this context, CrN coatings in our study were elaborated using pulsed DC magnetron sputtering as a PVD technique.

Hybrid duplex coatings combining thin films deposited by Physical Vapor Deposition PVD and Atomic Layer Deposition ALD are widely attracting attention as efficient surface protection technique. This is mainly due to specific improvements and enhancements in mechanical and corrosion properties [16–18]. Recent research works are focusing on the development of PVD+ALD multilayers coatings in order to limit corrosion damages.

Recently, Atomic Layer deposition ALD thin films are used as sealing [11], [19] or top layers [20–22] to improve corrosion and mechanical properties of PVD grown CrN layers. ALD is a unique deposition technique for growing thin films destined for microelectronics industry. ALD consists on saturating substrates surface by the reaction with two or more gaseous

precursors injected in separated pulses. Precursors-Substrate surface reaction is isolated by inert gas purge between two different precursors pulses. Nowadays, ALD thin films are showing promising results in high precision corrosion protection for metallic parts, steels and stainless steel systems. ALD process is based on the special mechanism of cyclic repetition of self-limiting surface reactions, which allows the unique control of the film thickness down to a molecular level [23–25]. In addition, ALD allows a conformal and uniform thin film growth on substrates in high aspect ratio and high quality permeation barrier layer. The low defects density in ALD films makes them the ideal choice as a barrier and sealing layer for blocking totally or as a wall-bottom conformal coverage of the PVD coatings pinholes and structural defects [26]. Several types of ALD thin films were studied in order to improve CrN coatings properties. Shan et al. [20] found that ALD-TiO_2/Magnetron sputtered CrN/Stainless steel double layer improved the corrosion resistance as compared to single layered CrN. Härkönen et al. [22] sealed the defects in hard CrN coating deposited on low alloy steel using 50 nm thick ALD Al_2O_3−Ta_2O_5 nanolaminate, $Al_xTa_yO_z$ mixture and $Al_xTa_yO_z$ graded mixture. They reported that the ALD layers had smoothen the overall appearance and decreased the size and number of pinhole defects on the surface. The combination of Al_2O_3 and Ta_2O_5 in the sealing layers had shown an increasing in barrier properties as validated by the polarization measurements where the current density was decreased by over 2 orders of magnitude. The long term durability is validated by Neutral Salt Spray NSS durability tests where the appearance of first corrosion spots was delayed from 2 to 168 h. They have combined the barrier properties of Al_2O_3 with the chemical stability of Ta_2O_5. Wan et al. [11] have demonstrated in their study that the addition of a dense atomic layer deposited Al_2O_3 interlayer maintains the mechanical properties of CrN coatings and leads to a significant decrease in the average grain size and surface roughness and thus greatly improving their corrosion resistance and durability. Leppäniemi et al. [21] sealed hard CrN/HSS (High Speed Steel) coating pinholes with ALD Al_2O_3/TiO_2 nanolaminate. They decreased the corrosion current density by approximately two orders of magnitude. Wan et al. [18] compared the influence of Al_2O_3, TiO_2, and Al_2O_3/TiO_2 nanolaminates as different ALD sealing layers on CrN coating. Their results have shown that nanolaminate Al_2O_3/TiO_2 sealing layers present the best corrosion performance with the highest corrosion potential and the lowest current density in both potentiodynamic and potentiostatic polarization tests compared to TiO_2 or Al_2O_3 sealing layers. It is due to the synergistic effect of the high electrical resistivity of Al_2O_3 with the high stability of TiO_2 in aqueous corrosive media. In another study, Leppäniemi et al. [26] investigated the effect of surface wear on corrosion protection of HSS by hybrid CrN/Al_2O_3-TiO_2 nanolaminates. Their results showed

that even with complete removal of the ALD nanolaminate from the top, the corrosion current density was less than half of that with the PVD CrN coating without surface wear. This validates the hypothesis that the excellent corrosion protection by hybrid PVD/ALD coating is due to PVD pinholes sealing by the ALD coating. Recently, Kong et al. [19] sealed CrN coatings with TiO_xN_y-TiN composite layer consisted of atomic layer deposited TiN bottom layer and TiO_xN_y upper layer synthesized by the oxidization of TiN layer in air. Therefore, the combination of properties of TiO_xN_y, which can block the charge transport and decrease the corrosion current between the corrosion interfaces, with the excellent sealing property of TiN improves the corrosion resistance of CrN coated steel. Furthermore, Kong et al. [17] reported the influence of TiO_2 and HfO_2 composite oxides on the microstructure, mechanical, tribological and electrochemical corrosion properties of CrN coatings. Meanwhile, due to the synergistic effect between the chemical durability of TiO_2 and the barrier properties of HfO_2, the TiO_2-HfO_2 nanolaminate-inserted CrN delivered excellent corrosion protection properties and displayed improved tribological properties.

Among all these ALD thin films, Al_2O_3 is validated [11] as an excellent insulating barrier film that could effectively enhance corrosion resistance of CrN on steel by blocking the diffusion of corrosive substances. Unfortunately, it needs to enhance its long-term durability against chemical attacks because its apt to dissolution [27] in water conditions, with an average dissolution rate that can reach up to 7 ± 1 nm/h in neutral NaCl solution [28]. However, thanks to its ability to nucleate on many kinds of surfaces, Al_2O_3 was usually used to reach up the drawbacks of many ALD films that present weak nucleation [29]. The optimized combination of Al_2O_3-MeO_x nanolaminates provides an improvement in corrosion protection [29], and good barrier properties with sufficient durability against chemical attack. In this study, we aim to investigate the effect of Al_2O_3-ZnO nanolaminates on mechanical and corrosion properties of CrN coatings deposited on 316L stainless steel.

Zinc oxide (ZnO) [30] is an n-type semiconductor with a wide band gap (3.36 eV) making it an important optoelectronic material with unique high thermal stability, catalytic and photo electronic properties. Hence, it is used for numerous applications [31], [32] in devices such as biosensors [33] and solar cells [34]. ALD is used to deposit ZnO films using diethyl zinc DEZ $Zn(C_2H_5)_2$) and deionized water vapor. Relatively, the corrosion behavior of ZnO ALD films to protect metals, including copper and stainless steel, has been evaluated. Thick ZnO coatings on copper [35] have shown a decreased corrosion current density, which initiated the use of

ZnO for corrosion applications [36]. According to Daubert el al. [35] 50 nm of thickness will improve the uniformity of ZnO thick films by decreasing porosity and would achieve high corrosion protection on copper. Therefore, increasing the thickness above 50 nm was not found useful and did not increase corrosion resistance. In order to compare different ALD thin films for their corrosion resistance, a 50 nm film is used as a model to accurately represent the corrosion properties of the ALD material. Staszuk et al. [37] studied the electrochemical properties of ZnO films on Cr-Ni-Mo steel and found that it has improved the resistance to corrosion damage of the tested material, which was evidenced by the increasing values of the corrosion potential and polarization resistance. Staszuk et al. [4] studied the effect of ZnO ALD layer on the adhesion of (Ti,Al)N Cathodic Arc Evaporation CAE-PVD coating on sialon substrates. The wear volume of the (Ti,Al)N/ ZnO coating was about three times lower than that of the (Ti,Al)N coating. The addition of ZnO layer led to a much better adhesion to the substrate as well as a higher abrasion resistance.

In ALD deposition, ZnO grows as a crystalline film [38], while Al_2O_3 is amorphous. Al_2O_3/ZnO nanolaminates [38] were investigated in many studies as well as their optical, mechanical, gas barrier and cytotoxicity properties. Herrmann et al.[39] and Raghavan et al. [40] studied the mechanical properties of Al_2O_3, ZnO and Al_2O_3 / ZnO nanolaminates. Al_2O_3 deposited by ALD presented a modulus of elasticity between 150 and 155 GPa and a hardness of 8 GPa, while ZnO deposited by ALD indicated a modulus between 120 and 140 GPa and a hardness of 5 GPa. The Al_2O_3 / ZnO nanolaminates exhibited a modulus of 140 to 145 GPa, which lies in between the value for the two films, and a hardness of 8 GPa, which is similar to that of Al_2O_3. Osorio et al. [41] examined the electrochemical behavior of these nanolaminates on 316L SS. Their results showed that the corrosion resistance of [Al_2O_3/ZnO]n nanolaminates was higher in comparison with single layered 316L SS surface. This confirms their protective effect against corrosion with higher polarization resistance. This improvement result was attributed to the decrease in the ZnO crystallites size with a higher number of multilayers, and therefore increasing the total number of grain boundaries in ZnO. It would be interesting to show how these materials can be approached and what are their limits in corrosion protection.

Following the positive results obtained in the previous articles, the present work aims to study the effect of Al_2O_3/ZnO ALD thin films on the mechanical and long-term protection against corrosion of CrN-coated 316L SS. A comparison between Al_2O_3, ZnO and Al_2O_3/ZnO ALD layers is evaluated. For the goal to achieve better performance of coating, a comparison

between three architectures forms of hybrid PVD+ALD combination is investigated: Substrate/PVD/ALD, Substrate/ALD/PVD and Substrate/PVD/ALD/PVD.

2. EXPERIMENTAL PROCEDURE

2.1. Substrates Preparation.

Quenched AISI 316L stainless steel disks (Φ 25 mm x 8 mm, purchased from UGITECH providers) and Single crystalline Si (100) wafers were used as substrates for coating deposition. 316L substrates were mechanically polished using SiC abrasive papers from 80 to 4000 grit followed by water based diamond suspensions of 3 µm and 1µm respectively in order to obtain an average roughness of Ra=50 nm. **Table 1** presents the chemical composition of 316L SS. The pitting resistance equivalent number PREN= 26.63. All the substrates were cleaned and degreased ultrasonically in acetone and ethanol for 10 min, and then, dry heated before deposition.

Table 1. Chemical composition of 316L quenched steel substrates.

Chemical Element	Fe	Cr	Ni	Mo	Mn	C
at%	balance	17.63	14.63	2.73	1.80	0.02

2.2. CrN coating deposition

Usually, a Cr layer should be deposited before any CrN films in order to enhance adhesion and tribological properties but this step was skipped in our study because we did not want to introduce any influencing process that could alter our comparison analysis. Our focus is to compare the adhesion properties that are directly related to the layers configuration in the S/ALD/PVD or the S/PVD/ALD architecture.

A DEPHIS4 (France) magnetron sputtering machine was used for CrN films elaboration. Prior to the deposition, the Chromium target (99.99 % purity, Φ=200 mm x 6 mm) was etched in Ar^+ bombardment (0.30 Pa, Argon flow rate = 100 sccm) to eliminate surface oxides, by applying a discharge power of 1A for 20 min. For all experiments, the target used was fixed at the same position in the chamber, its distance to substrate-holder was kept at 100 mm and substrates were fixed at the same zone on the substrate-holder. The deposition chamber was under vacuum, down to 10^{-6} mbar. CrN films were deposited at floating temperature using a mixture of Argon and Nitrogen gases injected in the chamber at 0.30 Pa. Elaboration conditions were summarized in **Table 2**. The substrate-holder rotation speed was set to 10 rpm. During deposition, no bias or substrates heating was performed. The thickness of the CrN layers was controlled by the modifying deposition time.

Table 2. CrN deposition parameters.

Target	Current [A]	Voltage [V]	Power [W]	Frequency [KHz]	Reverse Time [µs]
Cr	1.5	280	420	50	4
Working pressure 0.30 Pa					
Ar flow = 70 sccm ; N_2 flow=30 sccm					

2.3. Al_2O_3, ZnO and Al_2O_3/ZnO nanolaminates atomic layer deposition

A custom-made ALD reactor was used for thin films elaboration. Al_2O_3 layers were deposited by ALD process at 150°C using trimethylaluminium (TMA, Al $(CH_3)_3$) 98% purity, CAS: 75-24-1 was purchased from Sterm Chemical and H_2O as precursors. Each Cycling sequence consists of 0.2 s pulse of TMA, 30 s purge Ar, 2 s pulse H_2O and 40 s purge Ar. ZnO thin films were performed at 150°C using diethylzinc (DEZ, $Zn(CH_2CH_3)_2$, 95% purity, CAS: 557-20-0) and H_2O as precursors. ZnO regime consisted of 0.4 s pulse DEZ, 30 s purge Ar, 2 s pulse H_2O and 40 s purge Ar. Al_2O_3/ZnO nanolaminates were obtained by repeating sub cycles of Al_2O_3 and ZnO whereas the thickness of each unit cycle was fixed at ~ 2 nm for both. All ALD layers have the same thickness of 50 nm, corresponding to 250 cycles of Al_2O_3, 250 cycles for ZnO and 12*(10 cycles of Al_2O_3 + 10 cycles of ZnO) for nanolaminates respectively.

2.4. PVD/ALD, ALD/PVD and PVD/ALD/PVD architecured coatings elaboration

A 50 nm thick layer of Al_2O_3, ZnO or Al_2O_3/ZnO was respectively deposited on CrN layers for PVD/ALD configuration and as sealing layers for PVD/ALD/PVD configuration. In reverse, the CrN layers were deposited on these different ALD layers for ALD/PVD configuration. **Table 3** summarizes all the coatings elaborated with different architectures named with different numbers for more simplification. **Figure 1** represents a schematic illustration of these architectures.

Table 3. Coatings' architectures.

Sample No:	Architecture	Layers	Thickness
0 #	PVD	CrN	2.5 µm
1 #	ALD/PVD	Al_2O_3/CrN	50 nm/ 2.5 µm
2 #	ALD/PVD	ZnO/CrN	50 nm/ 2.5 µm
3 #	ALD/PVD	$[Al_2O_3\text{-}ZnO]_n$/CrN	50 nm/ 2.5 µm
4 #	PVD/ALD	CrN/ Al_2O_3	1.5 µm/ 50 nm
5 #	PVD/ALD	CrN/ZnO	1.5 µm/ 50 nm
6 #	PVD/ALD	CrN/$[Al_2O_3\text{-}ZnO]_n$	1.5 µm/ 50 nm
7 #	PVD/ALD/PVD	CrN/ Al_2O_3/CrN	1.5 µm/ 50 nm/1µm
8 #	PVD/ALD/PVD	CrN/ZnO/CrN	1.5 µm/ 50 nm/1µm
9 #	PVD/ALD/PVD	CrN/$[Al_2O_3\text{-}ZnO]_n$/CrN	1.5 µm/ 50 nm/1µm

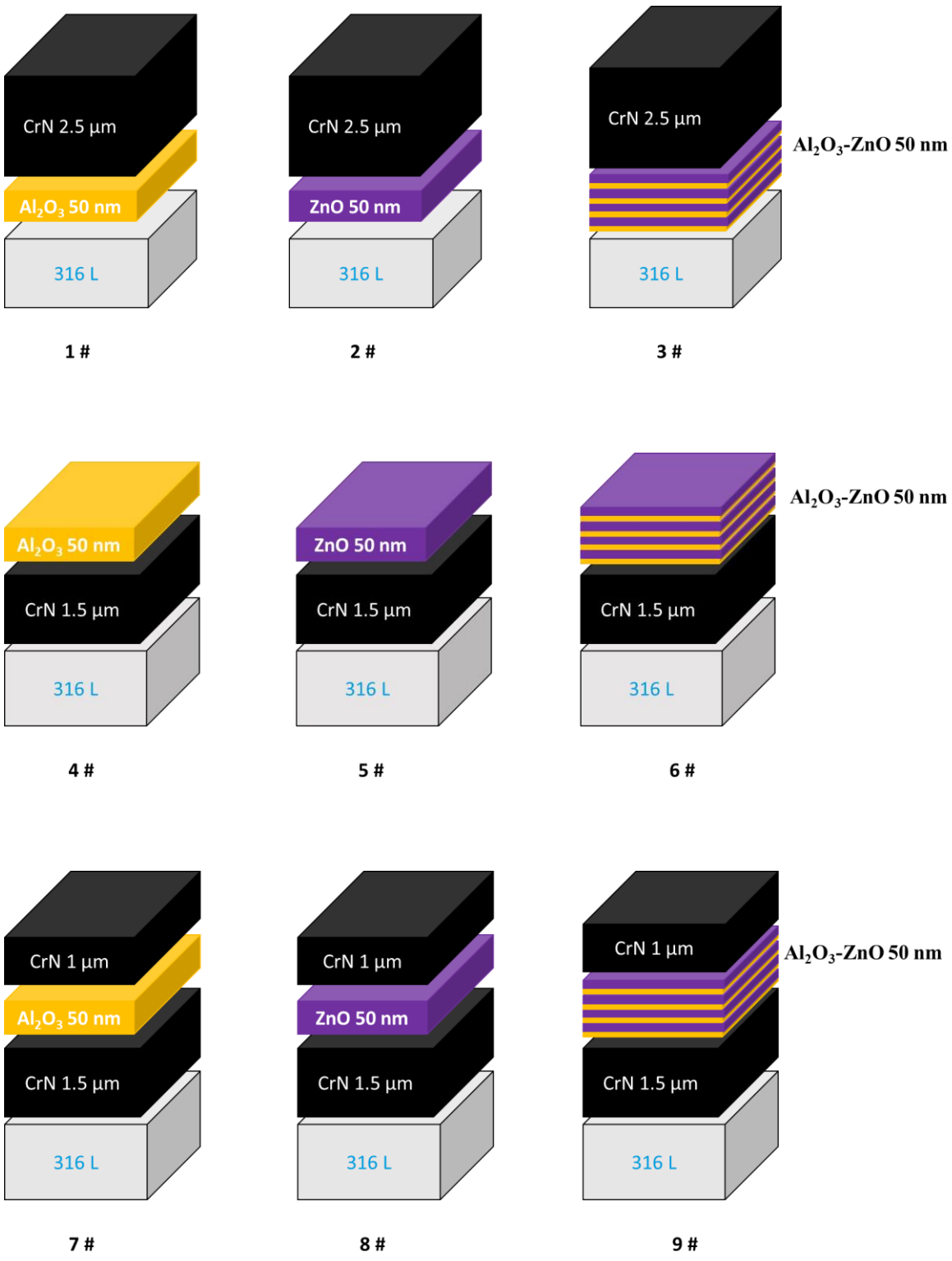

Figure 1. Schematic representation of different coatings architectures.

2.5. Coatings morphology, microstructure, chemical analysis, electrochemical and mechanical Characterization

FEG Hitachi SU 8030 Scanning Electron Microscope (SEM) was used was used to observe the coatings morphology and thicknesses. Chemical composition was determined using the scanning electron microscopy (SEM) Hirow SH-4000 M equipped with an X ray energy dispersive spectroscopy (EDS). Surface topography was determined using Bruker atomic force microscopy AFM. Scan zones were 2x2µm^2. Rms Roughness were calculated from AFM images using Nanoscope Analysis software. ImageJ software was used for top of column pyramidal particles size calculation from SEM images. Microstructure and crystal phases were identified by X-ray diffractometer (Bruker D8 advance, XRD) with Cu-Kα radiation (λ=1.5418 Å), operated at 40 kV and 40 mA. A θ-2θ scanning mode using a Bragg-Brentano configuration was performed for all samples measurements between 30° and 90° with a scan step of 0.02° and a step time of 1s. A 1 mm collimator was used for the incident beam. Full width at half maximum were determined after fitting the peaks using PseudoVoigt 1 function. Crystallite size were determined using Scherrer's formula:

$$D = \frac{k\lambda}{B\ cos\theta} \qquad \text{(Eq. 1)}$$

Where λ is wavelength of the X-rays used, k=0,94 is a correction factor, θ is the diffraction angle, B is the full width at half maximum (FWHM) of the film.

The texture coefficient for any reflection can be determined using the following relation:

$$TC = \frac{Im\ (hkl)/I0(hkl)}{(1/n)\sum\{Im(hkl)/I0(hkl)\}} \qquad \text{(Eq. 2)}$$

where n, the number of peaks; I_m, the measured peak intensities of reflections of CrN films; and I_0, the respective peak intensities corresponding to the bulk CrN data from JCPDS File No. 11-0065.

Hardness and reduced Young's modulus were measured using nanoindentation technique TriboIndenter TI 980-Hysitron equipped with a Berkovich diamond tip (E_{ind} = 1140 GPa, υ_{ind} = 0.07). In order to minimize the influence of substrate stiffness, the maximum of penetration depth is limited to lower than 10 % of the film thickness. Thirty indents were

performed for each sample and average values were taken into consideration. The uncertainty on measurements was determined from standard deviation. Contact angles were measured using Dataphysics OCA series machine based on sessile drop method. Droplet profile was acquired using a camera aligned with the samples and a backlighting source. Surface energy estimation was determined using Owens, Wendt, Rabel & Kälble (OWRK) method, with contact angles measured with the three liquid Water, Thiodiglycol and Diiodomethane. Five measurements with every solution were carried to ensure the reliability of data and only average values were taken into consideration.

The electrochemical corrosion properties of specimens were evaluated using Origalys potentiostat and Biologic flat corrosion cell adapted to samples dimension. Pitting corrosion was studied in 3.5 wt.% (0.6 M) NaCl solution, pH=6.3 at room temperature. Surface exposed for tests was limited to 1 cm^2. Corrosion system is based on conventional three electrodes. The saturated calomel electrode SCE (Hg/Hg_2Cl_2-Sat.KCl), platinum mesh and 316L SS with or without coatings were used as reference, counter and working electrodes respectively. In order to ensure system stability, the open circuit potential OCP was measured for 60 min. Measurement range was fixed from -150 mV/free to 1.3 V/ref, with reverse scan direction to -150 mV/free. The scan rate was fixed to 0.5 mV/sec, the current threshold to 3 mA and the stop reverse current at -10 mA. Tafel extrapolation method was used in order to determine Ecorr and polarization resistance Rp described as:

$$Rp = \frac{\beta a.\beta c}{2.303\ (\beta a+\beta c)} \times \frac{1}{Jcorr} \qquad \text{(Eq. 3)}$$

where βa and βc are the inverse of the anodic and the cathodic branches slopes and Jcorr is relative to corrosion current density.

Coatings porosity was calculated using the following equation [42]:

$$P = \frac{Rp,s}{Rp,coating}\ 10^{-\left(\frac{\Delta Ecorr}{\beta a}\right)} \qquad \text{(Eq. 4)}$$

where P is the total coating porosity, Rp,s is the polarization resistance of the substrate, Rp, coating is the polarization resistance of the coated steel, ΔEcorr is the difference between the

corrosion potentials of the coated steel and the 316 L steel substrate, and βa is the anodic Tafel slope of the substrate.

3. RESULTS

3.1. Coating morphology and surface topography

The elemental composition of Cr and N obtained by EDS was normalized to 100 at %. N content was 48.9 ± 4 at.% and Cr content 51.1 ± 2 at.%. The elemental concentration ratio of N/Cr was 0.96 indicating that CrN stoichiometric phase was obtained.

The surface morphologies of the deposited coatings are shown in **Figure 2**. The CrN films deposited using pulsed DC magnetron sputtering (**Figure 2 a**) shows a surface that exhibits a pyramidal like structure. These pyramids correspond to the caps of the columnar grains indicating that the CrN exhibits a columnar growth. This pyramidal morphology is similar to the one reported by Tan et al. [13] on their CrN films elaborated by DC sputtering at 30% N_2. This structure presents voids, contains pores and leads to a coarse surface. These defects could connects the substrate to surrounding environments. Wan et al. [18] in their study enhanced the corrosion and mechanical properties of a similar pyramidal CrN structures. In our study, no bias voltage or heating in sputtering elaboration were used to avoid their effects on ALD layers and to prevent any change in their properties due to temperature. In general, an adhesion Cr layer is inserted to enhance the adhesion between the substrate and the CrN layer. In order to compare with S/ALD/PVD architecture, no adhesion layer was deposited in our work.

Figures 2 b), c) and d) present the top view of the surface of the three S/ALD/PVD architectures respectively S/Al_2O_3/CrN, S/ZnO/CrN and S/ [Al_2O_3-ZnO] $_n$/CrN coatings. Chromium nitride layers deposited on the three different types of ALD layers conserve their pyramidal structures as shown in the corresponding SEM images. This indicates that the ALD layers did not provoke a change in the growth type of the CrN deposited by PVD. The columnar growth is conserved as on 316 L SS, and no other morphologies or distinctive features are observed. Pinholes and pores are seen on all three coatings. According to Dai et al.[16], the size of the granular structure attributed to the caps of the columnar crystals correlates to the diameter of the columnar crystals. In this context, the size of the pyramidal particles is measured from the SEM images and presented in **Figure 2 k)**. The three coatings 1# - 3# present a decrease in the dimensions of the pyramidal caps comparing to sample 0 #. This implies that the column size decreases. This decrease is absolutely due to the ALD

layers. This result confirms the granular refinement obtained in other studies [11] where the ALD interlayer formed a modified surface to allow the creation of more nucleation sites during deposition of the CrN layer.

Figures 2 e), f) and g) present the surface morphologies of samples 4# to 6# with Al_2O_3, ZnO, and $[Al_2O_3\text{-}ZnO]_n$ deposited on CrN. The ALD layers grew uniformly and conformably on the pyramids of the CrN structures. No pyramids structures are observed anymore where the ALD layers cover the pyramids. Even the summits of the pyramids are well covered by the ALD layer and the particles presents spherical and granular shapes. No pores or pinholes are observed anymore which indicates that the ALD layer sealed the defects. The boundaries between particles are still observed. The ALD layers smoothen the surface appearance and entirely cover the pores walls and the exposed surface at the bottom. The holes become smaller giving similar results to those obtained by Härkönen et al.[22].

Figures 2 h), i) and j) present the morphologies of the second CrN layer in the S/PVD/ALD/PVD architectures for samples 7# to 9#. The 1µm CrN second layer was deposited by PVD on the hillocks surfaces (**Figures 2 e, f and g**). Pyramidal structures are observed in the three figures. The particles are tightly packed and compacted compared with those obtained in samples 0# to 3#. Voids between particles are less pronounced compared to the S/ALD/PVD architectures (**Figures 2 b, c and d**). Particle sizes decreased compared to sample 0 #. The observed pyramids in sample 0 # refer to 2.5 µm in thick CrN while in samples 7# to 9# they correspond to only the second 1 µm CrN layer. This phenomenon is due to the interruption of the continuous growth of the CrN layer in samples 7# -9# by the ALD interlayer. This decrease has a relationship with the thickness of the CrN layer according to the structural region model of the thick film growth [43] since the columnar crystal is cone-like growth structure. No obvious morphology changes were observed among the hybrid coatings with different ALD interlayers.

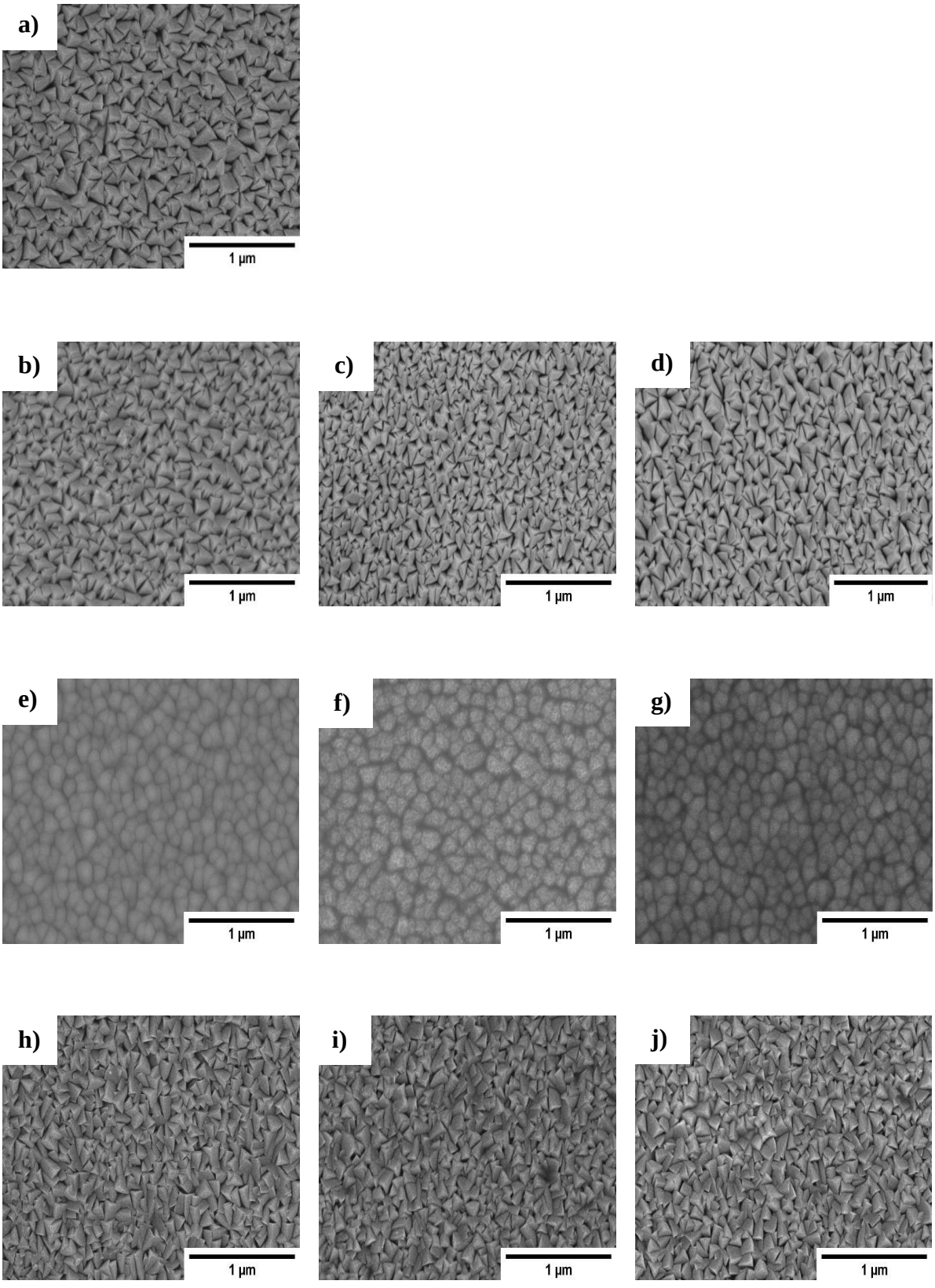
a)
1 µm
b)
1 µm
c)
1 µm
d)
1 µm
e)
1 µm
f)
1 µm
g)
1 µm
h)
1 µm
i)
1 µm
j)
1 µm

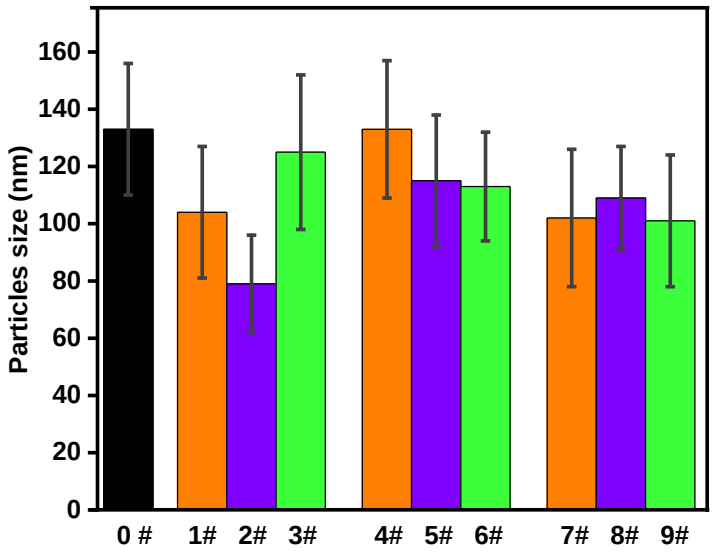

k)

Figure 2. SEM surface images of a) CrN , b) Al_2O_3/CrN, c) ZnO/CrN, d) [Al_2O_3-ZnO]$_n$/CrN, e) CrN/Al_2O_3, f) CrN/ZnO, g) CrN/[Al_2O_3-ZnO]$_n$, h) CrN/Al_2O_3/CrN, i) CrN/ZnO/CrN and j) CrN/[Al_2O_3-ZnO]$_n$/CrN; k) Histogram of particles sizes extracted from SEM images.

Root mean square surface roughness, *Rms*, represents a good approximation of surface height profile, with reduced contributions from large surface defects, for instance voids or micro-droplets [44]. **Figure 3** represents the AFM surface topography of specimen 0# to 9#. AFM images confirm all the surface morphologies observed in SEM top images (**Figure 2**). **Figure 3 k)** illustrates the variation of roughness of the different samples 0# to 9 #. The samples 1# to 9# indicate a decrease in the roughness compared to sample 0 #. This means that the ALD layer insertion, whatever the architecture is, smooths the surface and therefore decreases the roughness values. The samples 4# to 6# presents the higher decrease and the lowest roughness values compared to other samples. This is due to the architecture S/PVD/ALD where the ALD layer is on top, which smooths the surface roughness through an excellent compliance and uniformity over a large area. The decreased roughness in samples 1# to 3# and 7# to 9# is ascribed to the columnar refinement. Similar decrease in roughness is noted by Wan et al.[11] where in their study, the addition of the Al_2O_3 sealing layer by ALD decreased rapidly the roughness from 19.5 to 13.4 nm**.** Samples 1# to 3# in S/ALD/PVD architecture present higher roughness values than the samples 7# to 9# in S/PVD/ALD/PVD architecture. This is due to the higher density of voids in S/ALD/PVD architecture observed also in SEM surface analysis. Comparing the different ALD layers, $[Al_2O_3\text{-}ZnO]_n$ nanolaminates have the highest roughness regardless of the architecture, compared to Al_2O_3 and ZnO layers. This is due to the higher number of interfaces in the nanolaminate structure.

a) Rq= 34.5 nm

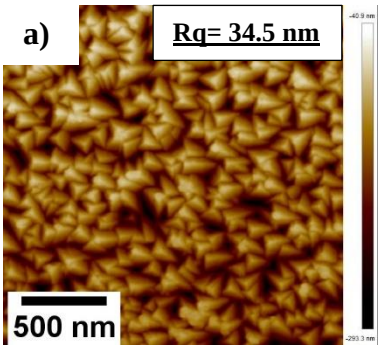

b) Rq= 23.5 nm

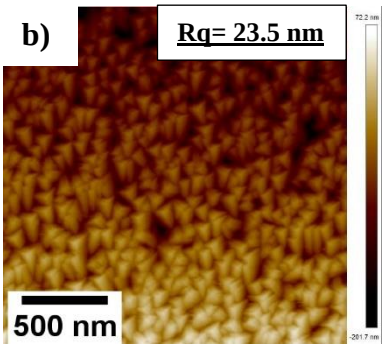

c) Rq= 24.5 nm

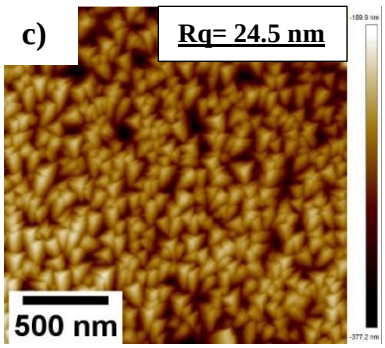

d) Rq= 28.6 nm

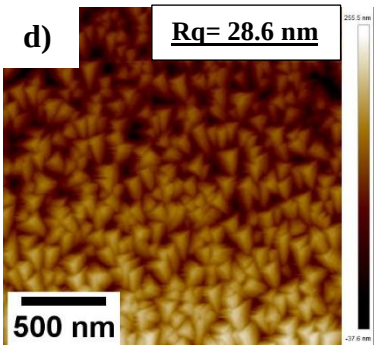

e) Rq= 17.2 nm

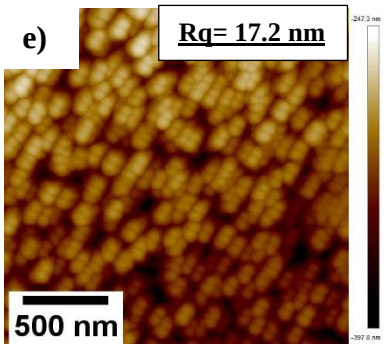

f) Rq= 13.8 nm

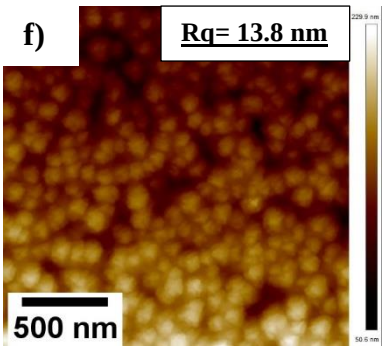

g) Rq= 16.8 nm

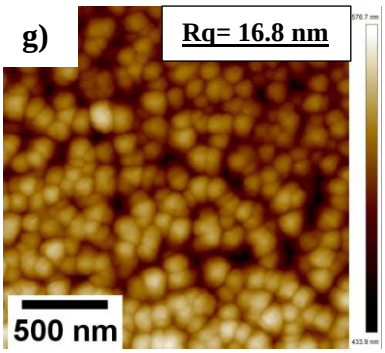

h) Rq= 18.5 nm

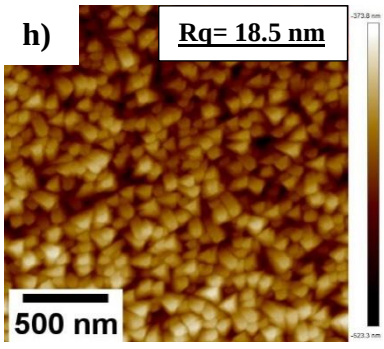

i) Rq= 18.3 nm

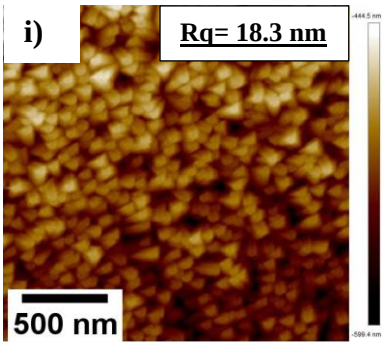

j) Rq= 20.4 nm

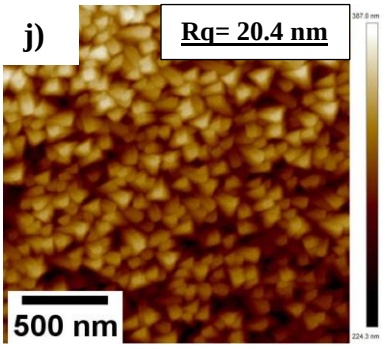

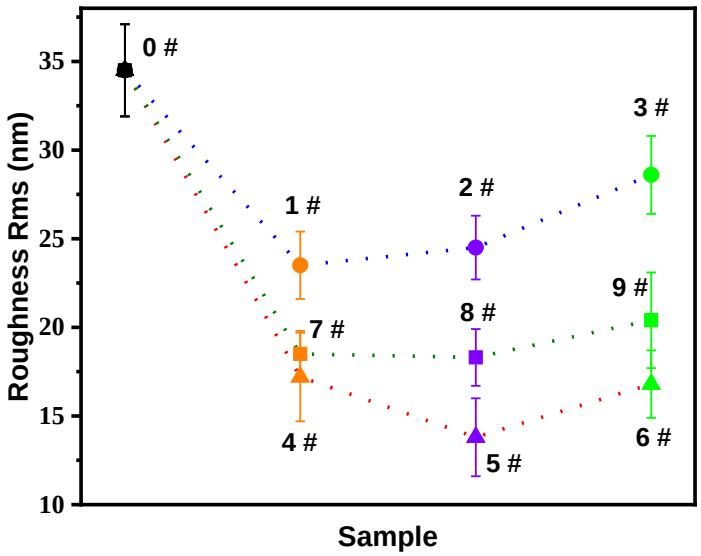

k)

Figure 3. AFM surface images of a) CrN , b) Al_2O_3/CrN, c) ZnO/CrN, d) $[Al_2O_3$-ZnO$]_n$/CrN, e) CrN/Al_2O_3, f) CrN/ZnO, g) CrN/$[Al_2O_3$-ZnO$]_n$, h) CrN/Al_2O_3/CrN, i) CrN/ZnO/CrN and j) CrN/$[Al_2O_3$-ZnO$]_n$/CrN; and k) represents the roughness variation of different samples.

Figure 4 represents the cross-section morphology of the coatings. All the coatings exhibit a columnar growth with 2.5 µm in thickness. **Figures 4 b), c) and d)** show finer columns diameter size than the sample 0 # that presents larger columns. They clearly show how the ALD layer is sandwiched between the substrate and the thicker PVD layer. The Al_2O_3 ALD layer shows a typical amorphous morphology. The ZnO layer shows a crystalline morphology high magnified in **Figure 4 k). Figures 4 e), f), g) and l)** show the 50 nm ALD layer on the top of 1.5 µm CrN layer. **Figures 4 h), i) and j)** show the insertion of ALD as a sealing layer between two PVD layers. There was a contrast difference in the CrN and the ZnO sealing layer in **Figure 4 i)** where a clear line was observed as ZnO layer. The inserted ALD layer interrupted the continuous growth, broke down the large columnar crystal growth and formed a modified surface to allow the creation of more nucleation sites during the deposition of CrN. Similar results are obtained with Wan et al.[11] in their study. **Figure 4 m)** shows the $[Al_2O_3\text{-}ZnO]_n$ nanolaminates inserted as sealing layer. These nanolaminates present a conformal growth between two CrN columns, combining two types of individual Al_2O_3 and ZnO sub-layers stacking together, could be evidently distinguished by the gray and white contrast, indicating the successful ALD deposition process and the progress of this experiment. The darkest zones reveal a lighter atomic weight corresponding to the Al_2O_3 layer.

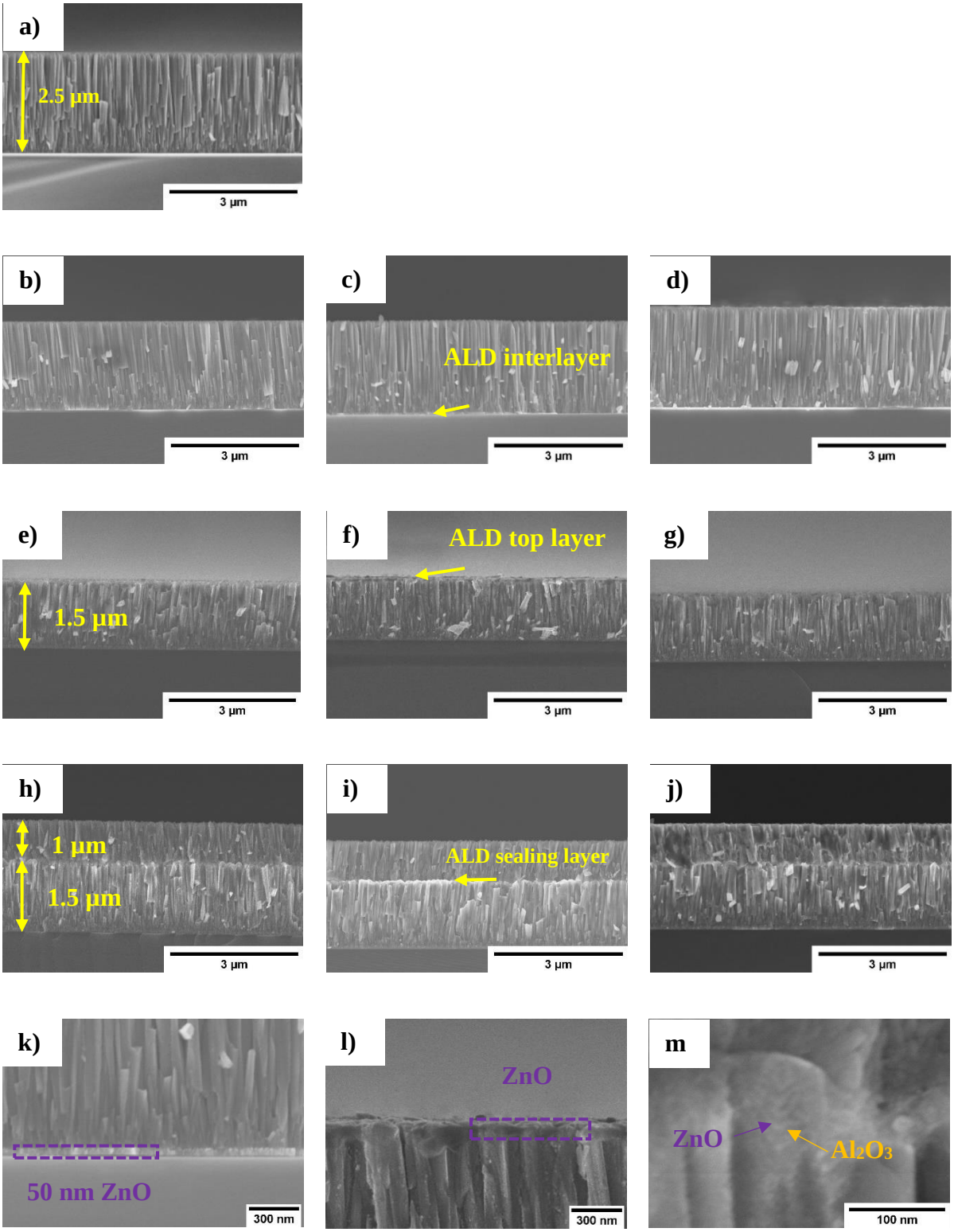

Figure 4. SEM cross section images of a) CrN, b) Al_2O_3/CrN, c) and k) ZnO/CrN, d)$[Al_2O_3$-ZnO$]_n$/CrN, e) CrN/Al_2O_3, f) and l) CrN/ZnO, g) CrN/$[Al_2O_3$-ZnO$]_n$, h) CrN/ Al_2O_3/CrN, i) CrN/ZnO/CrN, j) and m) CrN/$[Al_2O_3$-ZnO$]_n$/CrN.

3.2. Microstructure Analysis

XRD diffractograms of CrN and CrN+ALD coatings were shown in **Figure 5**. XRD patterns are organized per ALD layer material type in order to compare between the different architectures S/ALD/PVD, S/PVD/ALD and S/PVD/ALD/PVD. **Figure 5 a)** corresponds to Al_2O_3, **b)** to $[Al_2O_3\text{-}ZnO]_n$ nanolaminates, **c) and d)** to ZnO. XRD of CrN coating revealed a single NaCl type face centered cubic lattice with a preferred orientation of (111) plane. According to Tan et al.[13], in the DC conditions, the (111) orientations is the main preferred orientations, the CrN in our work sputtered in pulsed DC conditions exhibits also (111) preferential orientation. According to the standard reference file from the Joint Committee on Powder Diffraction (JCPDS, 11-0065), the three indexed peaks in the diffractogram at 2θ = 37.53°, 63.4° and 80.05° correspond to (111), (220) and (222) crystalline planes respectively. No traces of Cr_2N are detected due to the higher percentage of N_2 used during the deposition, at a floating temperature without heating nor bias voltage. The (220) peaks are almost undetectable. The peaks of CrN (200) and CrN (311) are not observed. The (200) orientation exhibits lower surface free energy while (111) orientation of CrN would be expected when the strain energy and the compressive stress in the films predominate [45]. The preferential orientation of our samples shows the advantage of simplifying the detection of the ALD influence on the texture of PVD coatings, and as mentioned in the literature by Ruden et al.[6], the coatings with preferential orientation in the (111) direction exhibit good anticorrosive behavior.

However, no diffraction peaks corresponding to the Al_2O_3 phase were detected, because it was deposited at low substrate temperatures (< 300 °C). Al_2O_3 is expected to be amorphous (**Figure 5 a)**. Weak XRD peaks at 2θ = 31.71°, 34.42° and 36.24° in **Figure 5 d)** (the magnified diffractogram of **Figure 5 c)** in 2θ range between 25° and 38°) correspond respectively to (100), (002) and (101) reflections of the wurtzite hexagonal ZnO layer. This indicates that the ZnO has a crystalline phase structure which is conform to literature [32]. The Al_2O_3/ZnO (2/2 nm) nanolaminates in **Figure 5 b)** did not show the ZnO peaks which could be attributed to their amorphous structure or their crystalline size below 2 nm as explained by Chaaya et al.[38].

The insertion of the ALD at any position did not provoke any phase transformation of the CrN matrix that is confirmed by no phase peaks detection for all duplex coatings. The inserted ALD oxide layer could result in enhancing the phase stabilization of CrN. All samples show the main diffraction peak around 37.5° corresponding to the CrN (111) and the peak at 80.05° relative to CrN (222). The (220) CrN peak is not detected in the S/ALD/PVD

architectures for the samples S/Al_2O_3/CrN, S/ZnO/CrN and S/ [Al_2O_3-ZnO]$_n$/CrN. It could be the result of the insertion of the oxide ALD layer that promoted the (111) textured orientation. The ALD layer altered the surface of the 316 L substrate, which now has different surface energy and different nucleation, and growth process of the PVD layer. Kong et al.[17] in their study observed that the insertion of ALD oxide interlayer leads to the CrN (111) textured orientation transformed from (111) and (200) planes and speculated that the ALD-oxide sealing layer could result in enhancing the phase stabilization of CrN. In another study, Kong et al.[3] noted that the preferred orientation of TiN transforms to (200) and (220) from the original (111) orientation after the addition of the ALD-Al_2O_3 interlayer. No such transformation in textures was observed in our study but a little variation was detected. To more investigate the texture variations, texture coefficient (TC) was calculated for the three orientations (**Table 4**).

Table 4 represents the lattice parameter, the crystallite size and the texture coefficient for the S/ALD/PVD and S/PVD/ALD/PVD samples. In the S/ALD/PVD architecture, the ALD promotes the (111) orientation. While in S/PVD/ALD/PVD architecture, the TC of (220) orientation shows higher values than TC=0.013 of the CrN layer (sample 0#). The grain size of the CrN film was calculated by Scherrer's formula. Calculated lattice parameter of CrN is 4.152 Å. All samples revealed an increase in the lattice parameter, which could be related to the insertion of the ALD-oxide layer that would effectively lower the residual stress of CrN coatings. All samples showed a decrease in crystallite size. Meanwhile, the ALD layer creates more nucleation sites that could suppress the large columnar crystal growth and contribute to crystal refinement.

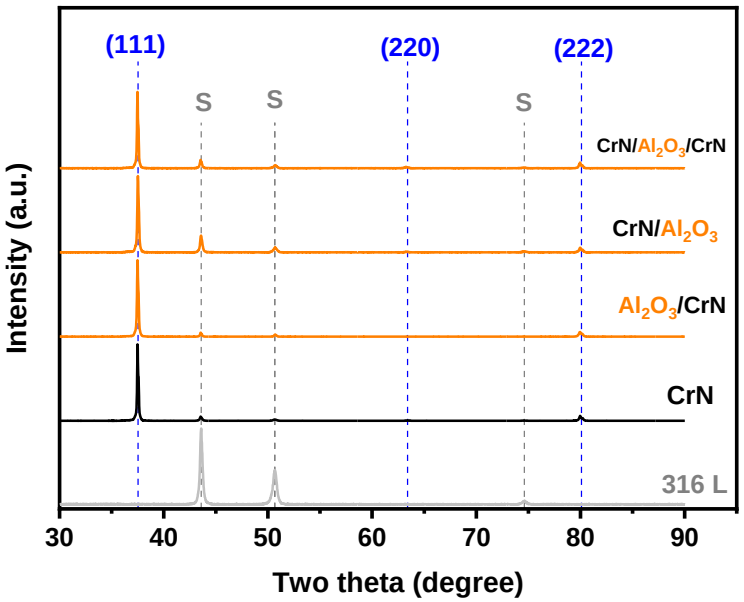
(111)
(220)
(222)
S
S
S
CrN/Al2O3/CrN
CrN/Al2O3
Al2O3/CrN
CrN
316 L
Intensity (a.u.)
30
40
50
60
70
80
90
Two theta (degree)

a)

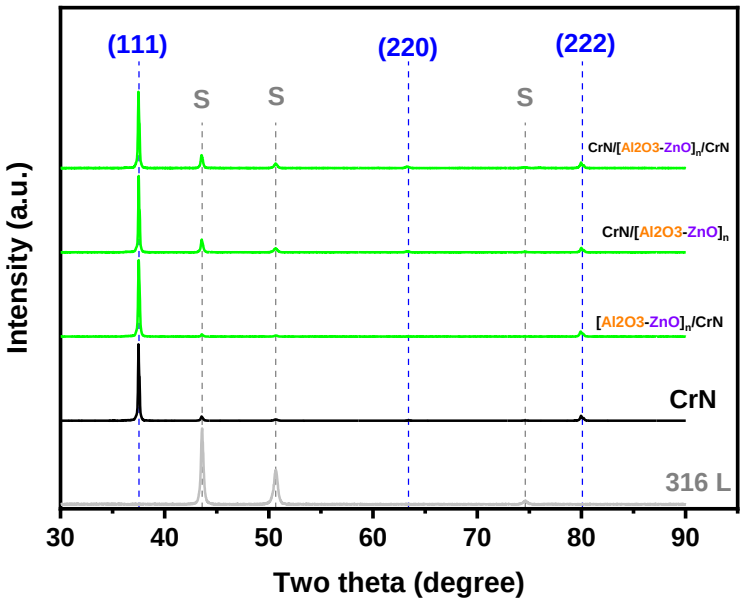
(111)
(220)
(222)
S
S
S
CrN/[Al2O3-ZnO]n/CrN
CrN/[Al2O3-ZnO]n
[Al2O3-ZnO]n/CrN
CrN
316 L
Intensity (a.u.)
30
40
50
60
70
80
90
Two theta (degree)

b)

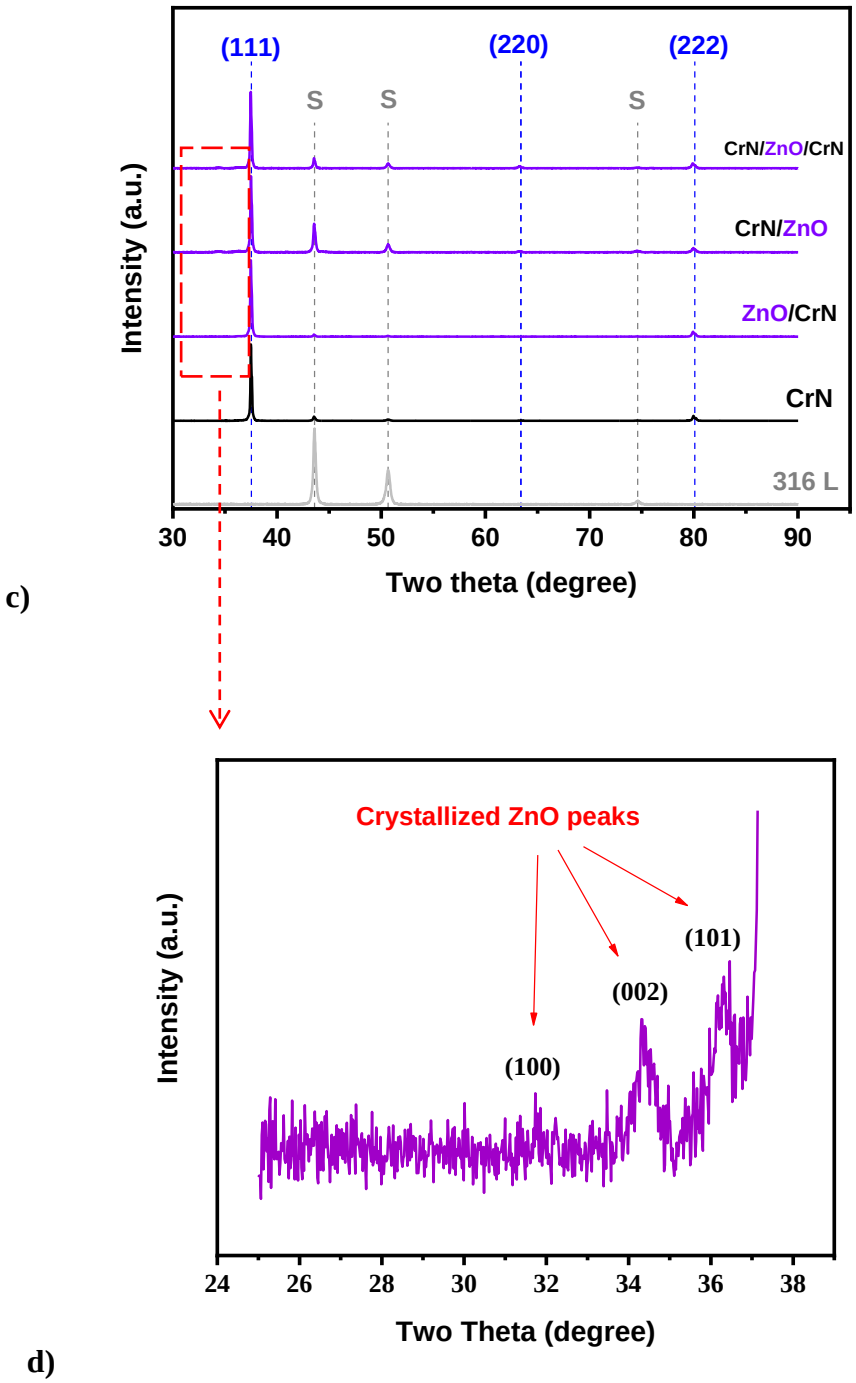

Figure 5. XRD diffractograms of a) samples 0#, 1#, 4#, 7# ; b) 0#, 3#, 6#, 9#; c) 0#, 2#, 5#, 8# and d) magnified zone of crystallized wurtzite ZnO phase peaks.

Table 4. Lattice parameter, Crystallite size and Harris texture coefficient of samples 0#-3# and 7#-9#.

Sample	**Lattice parameter a (Å)**	**Crystallite size (nm)**	**Harris TC**		
			(111)	**(220)**	**(222)**
0#	4.152	52.2	2.58	0.01	0.41
1#	4.153	48.4	2.63	-	0.37
2#	4.154	49.0	2.62	-	0.38
3#	4.153	47.9	2.62	-	0.38
7#	4.153	51.9	2.54	0.04	0.42
8#	4.156	51.3	2.54	0.06	0.40
9#	4.154	48.8	2.54	0.05	0.40

3.3. Mechanical Properties

Nanomechanical properties assessments are needed to develop a fundamental understanding of surface and interfacial phenomena on a small scale. Hardness represents the inherent resistance of the material to the elastoplastically deformation. It is known that several factors could affect the film hardness, such as residual stress, preferred orientation and grain size. Nanoindentation tests were carried out to evaluate the hardness and the elastic modulus of the coatings. Predicting elastic strain before plastic deformation, wear and plastic deformation resistances of the coatings are done by calculating the H/Er and H^3/Er^2 ratios. The mechanical properties are shown in **Figure 6**.

The as deposited chromium nitride presents a hardness of 5.3 GPa and a Young's modulus of 113 GPa. It is well known that chromium nitride films have a hardness of 18~21 GPa [46]. The relative low hardness and elastic modulus of the CrN coating in our study may be attributed to columnar structure of the film, the presence of voids and the absence of Cr_2N phase. It was mentioned that the presence of Cr_2N phase has a much higher hardness as compared to the films with a dominant CrN phase [47]. Similar low hardness ~8 GPa was observed with the CrN thicker than 2µm elaborated by Zairi [48].

All the samples present a higher hardness and Young's modulus compared to the as deposited CrN. This increase in hardness is due to the grain size refinement according to the Hall-Petch relation. The dense ALD layer with few defects is a good barrier layer for blocking defects proliferation and dislocation motion in the CrN layer during the indentation. The ALD layers resisted shear sliding between vertically aligned columnar grains, which enhanced the mechanical properties of the CrN coatings. Similar enhancement in mechanical properties is observed in other studies [11], [16], [17].

Figure 6 a) represents the mechanical properties of the S/ALD/PVD coatings. The insertion of Al_2O_3, ZnO or nanolaminates layers between the substrate and the CrN increases the hardness and the Young's modulus of CrN layer. The Al_2O_3 layer induced the highest increase, comparing to ZnO and nanolaminates. This difference could be due to the polycrystalline structure of ZnO and the intrinsic hardness of alumina. The $S/Al_2O_3/CrN$ architecture show a slight enhancement with a hardness value of 6 GPa and Er=131 GPa. H/Er and H^3/Er^2 ratios in **figure 6 b)** showed a decrease with the insertion of the ALD as an

interlayer between the substrate and CrN (except H^3/Er^2=0.013 GPa for Al_2O_3/CrN > 0.012 GPa for CrN). Meanwhile, the ALD insertion through the S/ALD/PVD architecture decreases the resistance to cracks initiation and propagation, the ability for elastic deformation and the wear resistance of the CrN layer.

Figures 6 c) and d) represent the mechanical properties of the S/PVD/ALD coatings. The nanoindentation penetration depth in these coatings exceeds 50 nm, so by reaching deeper than the ALD layer it measures the hardness and Young's modulus of both the PVD and the ALD layers. In S/ALD/PVD and S/PVD/ALD/PVD, H and Er are characteristics of the PVD layer only because the penetration depth do not reach beyond the top layer and the values give an idea on the ALD influence on the PVD. However, the values in S/PVD/ALD architecture characterize the coating as a system. These architectures present a higher improvement in mechanical properties. The hardness in S/CrN/Al_2O_3 increased to 11 GPa which is higher than CrN hardness by 2 orders of magnitude. Also, H/Er and H^3/Er^2 increased respectively from 0.047 to 0.082 and from 0.012 to 0.075 GPa in S/CrN/Al_2O_3. Meanwhile, S/PVD/ALD coatings are strength, wear and plastic deformation resistant. Al_2O_3 shows the highest improvement in mechanical properties.

Figures 6 e) and f) represent the mechanical properties of the S/PVD/ALD/PVD coatings. All the coatings showed an increase into order of 2 GPa to the hardness of CrN. H/Er and H^3/Er^2 ratios increased and the CrN/$[Al_2O_3\text{-}ZnO]_n$/CrN coating exhibits the highest improvement compared to samples 7# and 8#. Meanwhile, the $[Al_2O_3\text{-}ZnO]_n$ nanolaminates present a better enhancement than Al_2O_3 and ZnO. Herrman et al.[39] have determined the hardness of Al_2O_3 and Al_2O_3/ZnO nanolaminates by 8 GPa while ZnO presents a hardness of 5 GPa. It is known that the increment of interfaces in the case of multilayers results in higher hardness and elastic constant of the samples. However, the interfaces in Al_2O_3/ZnO nanolaminates allow the allocation of shear stress, which stops the propagation of cracks and, ultimately, prevents the failure of the films. We conclude that the nanolaminates structure is more effective in S/PVD/ALD/PVD architecture than others.

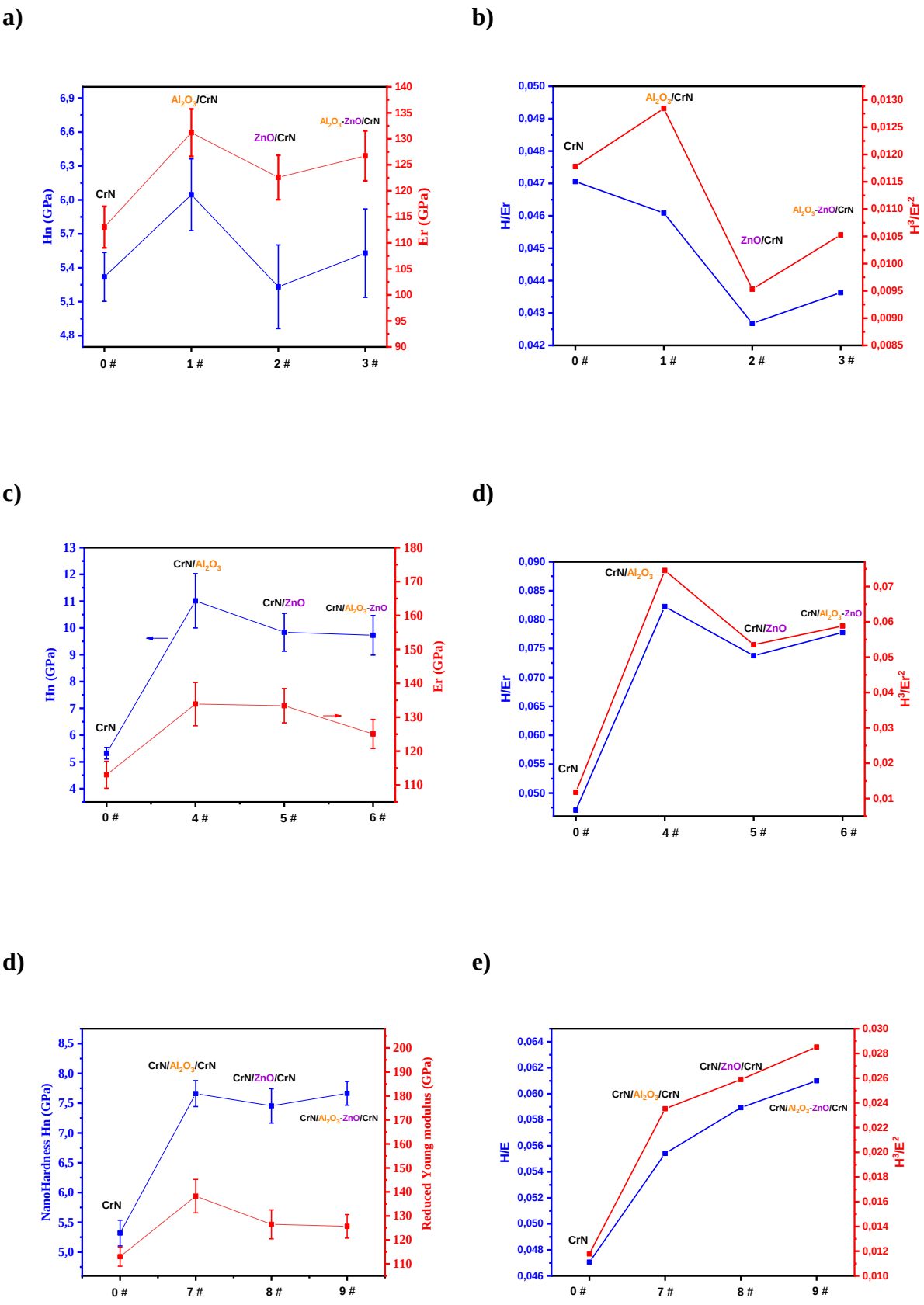

Figure 6. Mechanical properties of the coatings.

3.4. Surface wettability behavior

Contact angles measurements were carried out on the surface of the coatings at room temperature to study the interaction of the films with water and to determine their wettability behavior. **Figure 7** shows the images of contact angles of water droplets fallen down on the surfaces of the films, the variation on the different hybrid architectures and for the three different ALD layers. To our knowledge, no literature data on the wettability of ALD+PVD hybrid coatings is available. Chromium nitride thin films presents a contact angle CA= 18 ° which exhibits the hydrophilicity character of the film. The S/ALD/PVD coatings exhibit a hydrophilic character. This could be due to the surface of the PVD layer which is in contact with the surrounding environment. The high density of voids observed in the SEM images of these coatings would justify their hydrophilicity. We can conclude that the insertion of ALD layer between the substrate and the PVD layer has less influence on the wettability behavior of the PVD external layer. The S/PVD/ALD coatings exhibit a hydrophobicity character to water. They show a CA superior to 90°. This change of wettability compared to CrN is due to the ALD layer that controls the interaction of the coatings with the surrounding liquid and determines the wettability of the present coating. The S/PVD/ALD/PVD coatings exhibit a change in the wettability compared to CrN. The CrN/Al_2O_3/CrN presents a CA=68° which is higher than 18° of CrN. The CrN/ZnO/CrN and the CrN/$[Al_2O_3$-ZnO$]_n$/CrN have CA of 40° and 33° respectively. This change in wettability is due to the change in the second 1µm CrN layer and to the insertion of ALD sealing layers. The presence of the nucleation sites, which are attributed to the refinement of the CrN columns and to the reduction of voids density and the decrease in roughness, is the reason of the observed changes in wettability. **Figure 7 l)** represents the variation of the coating surface energy calculated using three liquids: Water, Thiodiglycol and Diiodomethane. Hydrophilic films exhibit higher surface energy and lower contact angle in comparison to the hydrophobic films.

a)

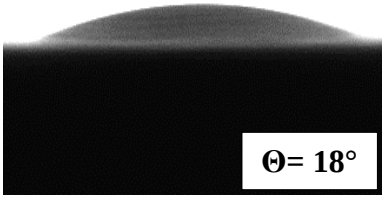

b)

c)

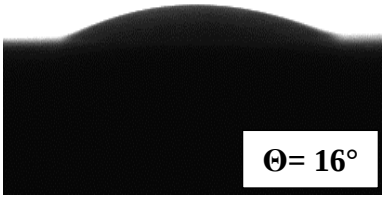

d)

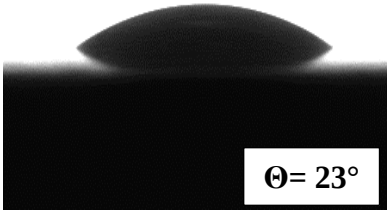

e)

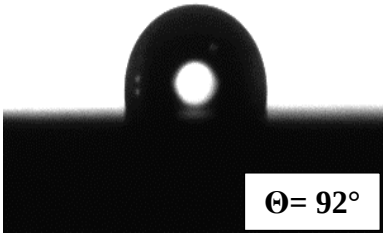

f)

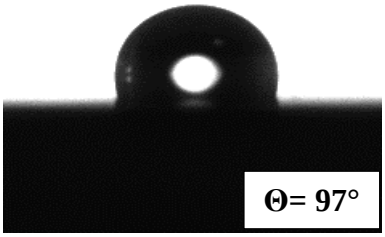

g)

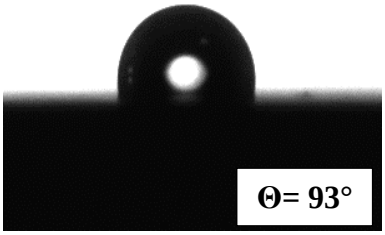

h)

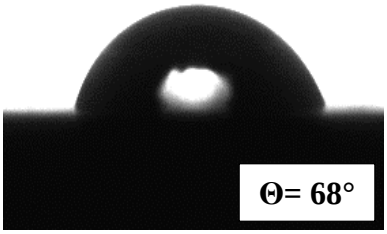

i)

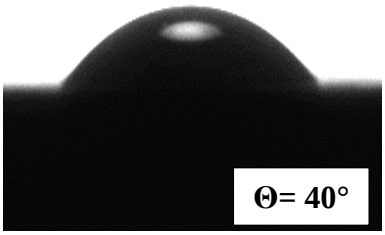

j)

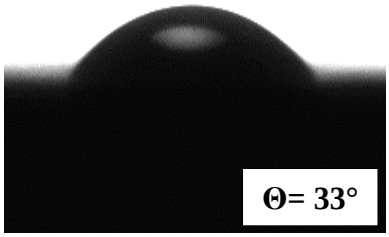

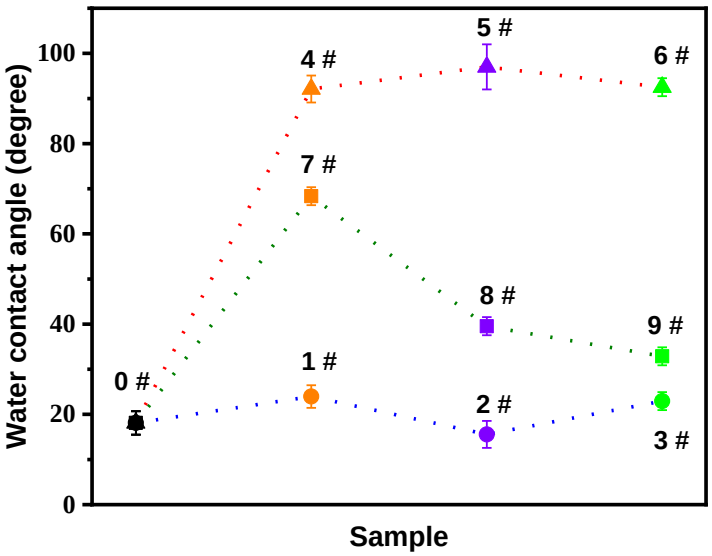

k)

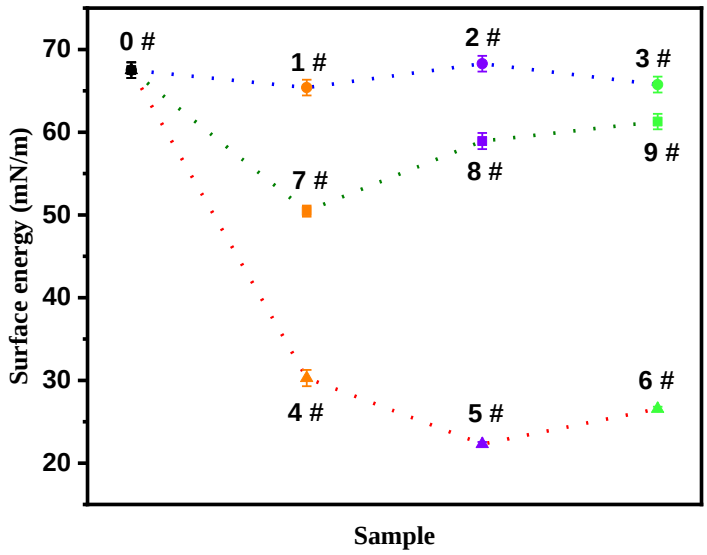

l)

Figure 7. Water contact angle of a) CrN; b) Al_2O_3/CrN; c) and k) ZnO/CrN; d)[Al_2O_3-ZnO]$_n$/CrN; e) CrN/Al_2O_3; f) and l) CrN/ZnO; g) CrN/[Al_2O_3-ZnO]$_n$; h) CrN/Al_2O_3/CrN; i) CrN/ZnO/CrN; j) and m) CrN/[Al_2O_3-ZnO]$_n$/CrN; k) Water contact angle and l) surface energy variations of the different architectured coatings.

3.5. Corrosion Behavior

The coatings corrosion behavior was characterized using cyclic polarization tests in saline solution as shown in **Figures 8**. **Table 5** represents the electrochemical parameters of the different samples. The corrosion current density i_{corr} was determined using Tafel extrapolation from the polarization curves by extending a straight line along the linear portion of the cathodic plot and extrapolating it to the E_{corr} axis due to the asymmetry of the polarization curve between the anodic and cathodic branches. E_{pit} represents the potential of pitting which corresponds to the breakdown of the passive film. The corrosion density is related to the corrosion rate.

The 316 L substrate present a low corrosion density due the formation of Cr_2O_3 passive film. As shown in **Figure 8 a)**, the polarization curve of the 316 L substrate presents current fluctuations between 200 and 400 mV corresponding to metastable pits and re-passivation of the surface. The passive film breaks down totally and leads to the increase in current density and the formation of stable pits at 415 mV. The CrN coatings are known to be more noble than the steel and chemically inert [7]. In these samples the corrosion potential is shifted to higher values E_{corr}=57 mV and the pitting potential goes from 415 mV to 530 mV. A passive stage is observed between 50 and 500 mV vs SCE. The breakdown of the passive film indicates the formation of pits. The reverse scan of the polarization curve indicates that the coating does not exhibit any re-passivation. i_{corr} and R_p of the CrN are lower than those of 316 L substrate which is due to the columnar structure of the CrN, and the high density of voids and defects presented in this structure. CrN porosity is assimilated to be 1.6 E^{-02}, which is the highest between all the coatings.

The insertion of an ALD layer between the substrate and the CrN layer (S/ALD/PVD architecture) slightly shifts the CrN corrosion potential to higher values whatever the inserted ALD layer type is. As shown in **Figure 8 a)**, the insertion of Al_2O_3-ZnO nanolaminates interlayer shifts the E_{corr} to higher values than Al_2O_3 or ZnO. While ZnO and Al_2O_3 lead to a decrease in corrosion density, the S/$[Al_2O_3$-ZnO$]_n$/CrN presents a higher corrosion density and lower polarization resistance. This could be due to the higher porosities of this film, which exhibits also a higher roughness.

Figure 8 c) shows the polarization curves of the S/PVD/ALD architectured coatings. All the coatings exhibit a decrease in the corrosion potential. This could be attributed to the failure mechanism of corrosion protection of these ALD layers. The ALD is in such a position which enhances the direct interaction with the NaCl environments. These could facilitate the Cl^- ions attack to the ALD layer and accelerates its dissolution. Corrosion products and rusts modify the CrN underlayer composition and could accumulate in the bottom of some pinholes. Meanwhile, this could be the reason for potential shifts for lower values. However, the ALD nanolaminates in this architecture provide the higher protection efficiency compared to Al_2O_3 and ZnO. The samples had very low current densities and thus a significant amount of noise in the whole potential range measured. The corrosion density of S/CrN/$[Al_2O_3$-ZnO$]_n$ coating decreases from 285 to 0.6 $nA.cm^{-2}$. This means that the ALD nanolaminates structure decreases the corrosion rate. The 2 nm Al_2O_3 and ZnO alternating layers decreases the dissolution of ALD layers and it is more efficient in corrosion protection behavior. The reverse scan of this coating presents the ability to repassivation. Epit of S/CrN/$[Al_2O_3$-ZnO$]_n$ coating shifted to 947 mV vs SCE. This means that the S/CrN/$[Al_2O_3$-ZnO$]_n$ coating provides a protection against pitting. The insertion of an insulating Al_2O_3 layer between the n-type semiconducting ZnO layers leads to an architecture that varies the electric properties and charge conductivity. The nanolaminates acted as a perfect insulating barrier for blocking charge transport in the coatings and the current flow from the anode to the cathode, which decreased the corrosion current density and reduced the electron exchange rate and dissolution rate of the anode metal ions at the corrosion interface as explained by Wan et al. [11]. The hydrophobicity of these coatings attributes to the improvement the corrosion resistance.

The polarization curves of the S/PVD/ALD/PVD architectured coatings are shown in **Figure 8 d)**. Coatings having this architecture present the lower porosities, which means that the insertion of the ALD as a sealing layer is more efficient in decreasing the porosities than ALD in other structures. The dense ALD layer, with few defects, covers the walls and the bottom of the first PVD layer defects; then it contributes to the reduction of voids between the columns of the second PVD layer by creating more nucleation sites for the growth of refined columns. Furthermore, the ALD layer constitutes a good barrier for blocking the diffusion of corrosive substances, such as chlorine ions. The CrN/$[Al_2O_3$-ZnO$]_n$/CrN coating has a corrosion potential that lies between those of CrN/Al_2O_3/CrN and CrN/ZnO/CrN coatings. The shifts of E_{pit} values to the region of 720 mV vs SCE was observed in these

coatings along with a high decrease in the corrosion densities was noticed. The $CrN/Al_2O_3/CrN$ and the $CrN/[Al_2O_3\text{-}ZnO]_n/CrN$ coatings showed an ability to re-passivation in the reverse scans which means that these two coatings present higher protection against pitting corrosion. The $CrN/[Al_2O_3\text{-}ZnO]_n/CrN$ coating presents the best corrosion protection performance with the lowest $I_{corr} \sim 7.9 \times 10^{-10}$ A/cm^2 lower two order of magnitude than I_{corr} of the substrate $\sim 1.5 \times 10^{-8}$ A/cm^2.

Figures 8 e) f) and g) show the comparison between the different architectures for the same ALD layer. We can conclude that the S/PVD/ALD/PVD architecture is the most efficient architecture to provide an improvement in corrosion resistance. The surface images in **Figure 9** of the corresponding samples after corrosion tests were obtained using a profilometer altisurf. Pitting zones with large diameters were present on the CrN sample. The three samples S/ALD/PVD (1, 2 and 3#) showed a delamination of some zones of the CrN layer which is due to the anodic dissolution and the propagation of the pits. Sample 4# shows residual zones of dissolved Al_2O_3 layer and the damage of the CrN surface. Samples with ZnO layers 5# and 8# show high density of pits with lower diameter and some rusts were present on the surface. The $CrN/[Al_2O_3\text{-}ZnO]_n$ and $CrN/[Al_2O_3\text{-}ZnO]_n/CrN$ coatings presented the smoother surfaces without pits.

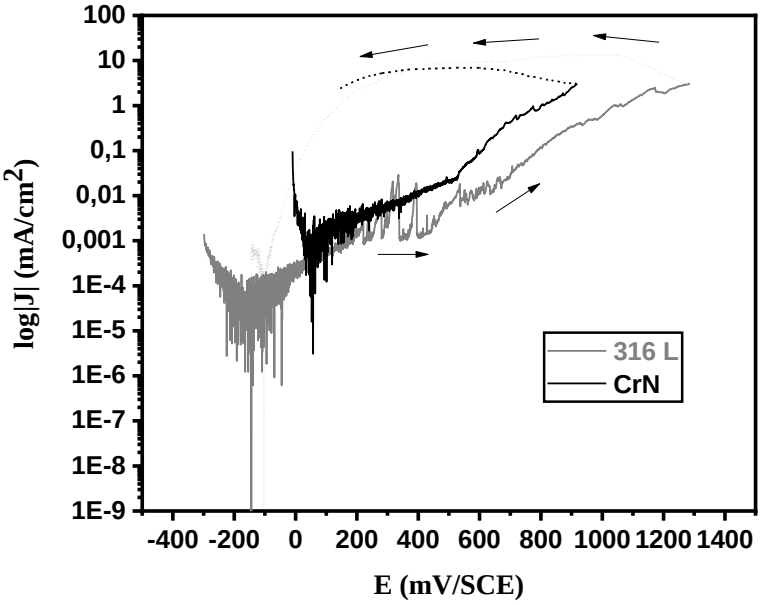
100
10
1
0,1
0,01
0,001
1E-4
1E-5
1E-6
1E-7
1E-8
1E-9
log|J| (mA/cm2)
-400 -200 0 200 400 600 800 1000 1200 1400
E (mV/SCE)
316 L
CrN

a)

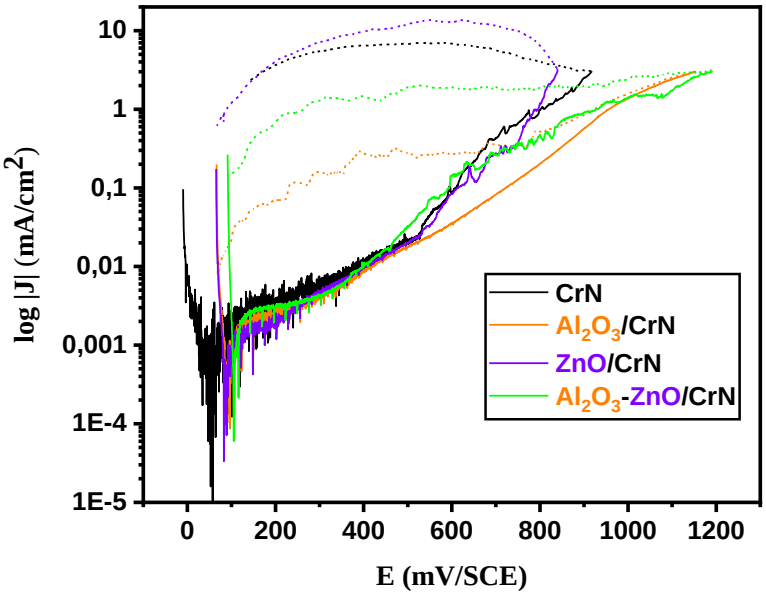
10
1
0,1
0,01
0,001
1E-4
1E-5
log |J| (mA/cm2)
0 200 400 600 800 1000 1200
E (mV/SCE)
CrN
Al2O3/CrN
ZnO/CrN
Al2O3-ZnO/CrN

b)

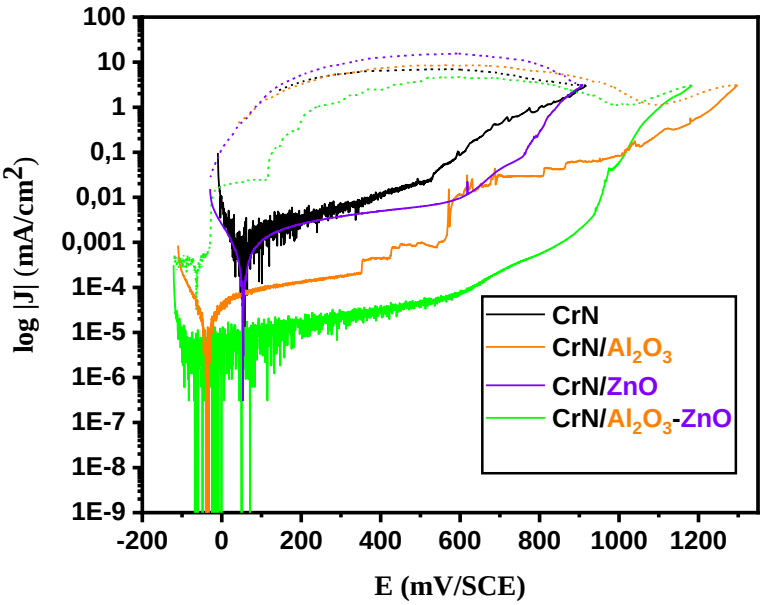
log |J| (mA/cm2)
E (mV/SCE)
CrN
CrN/Al2O3
CrN/ZnO
CrN/Al2O3-ZnO

c)

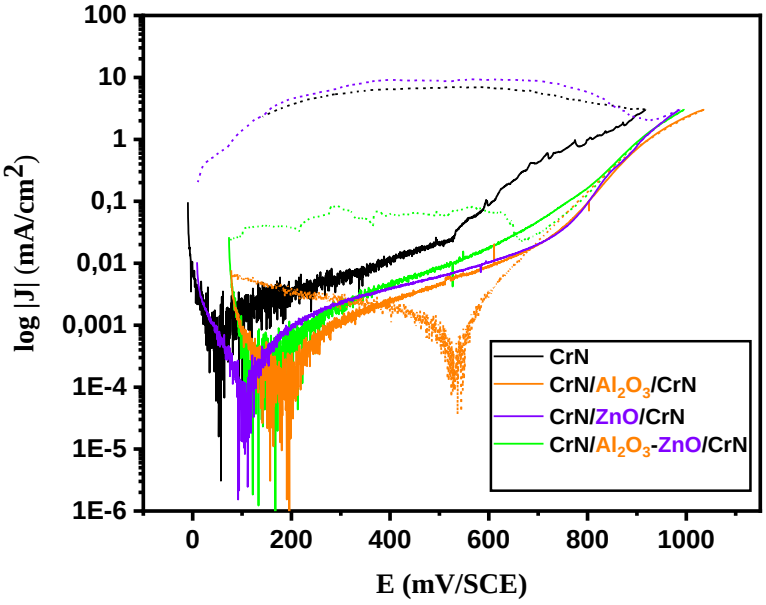
log |J| (mA/cm2)
E (mV/SCE)
CrN
CrN/Al2O3/CrN
CrN/ZnO/CrN
CrN/Al2O3-ZnO/CrN

d)

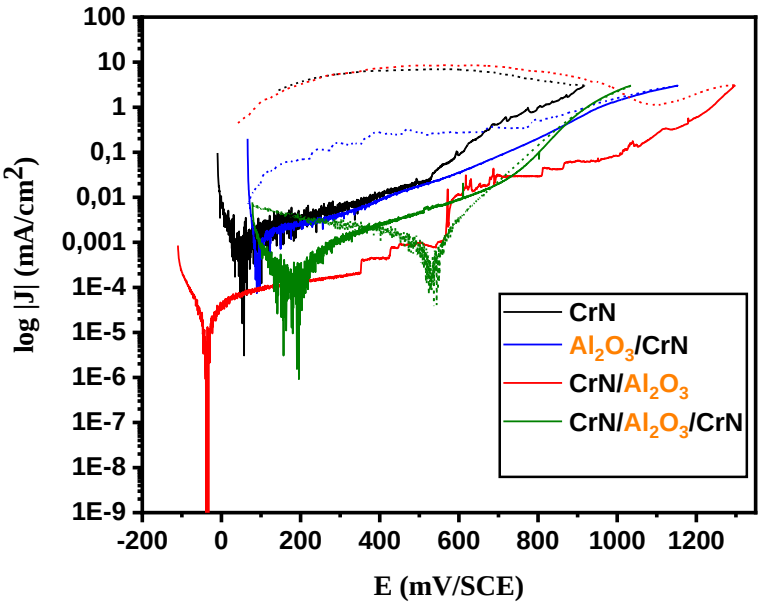
100
10
1
0,1
0,01
0,001
1E-4
1E-5
1E-6
1E-7
1E-8
1E-9
log |J| (mA/cm2)
-200
0
200
400
600
800
1000
1200
E (mV/SCE)
CrN
Al2O3/CrN
CrN/Al2O3
CrN/Al2O3/CrN

e)

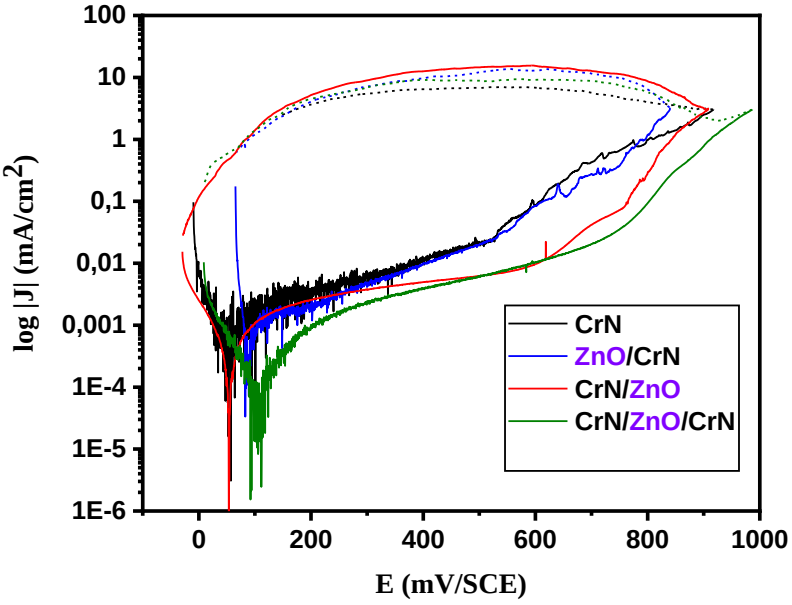
100
10
1
0,1
0,01
0,001
1E-4
1E-5
1E-6
log |J| (mA/cm2)
0
200
400
600
800
1000
E (mV/SCE)
CrN
ZnO/CrN
CrN/ZnO
CrN/ZnO/CrN

f)

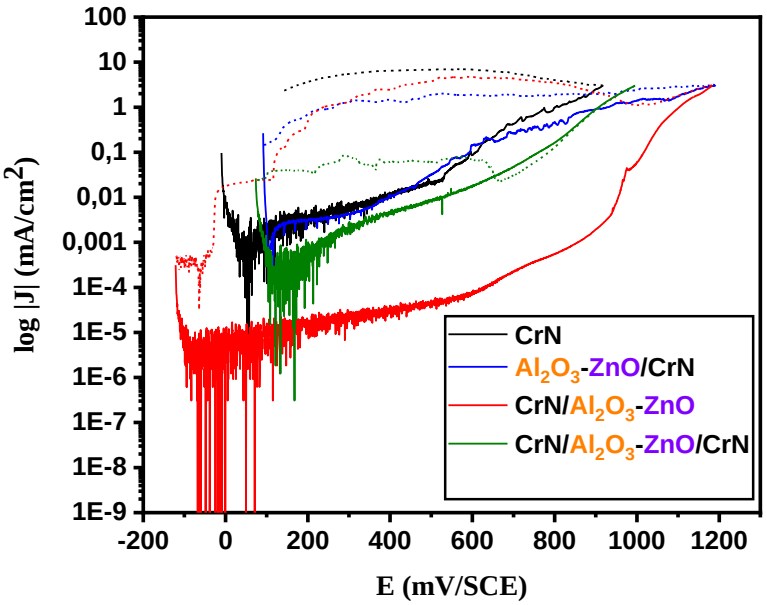

g)

Figure 8. Cyclic polarization curves in saline solution for coatings.

Table 5. Corrosion electrochemical parameters of the different samples.

Sample	*316L SS*	*0#*	*1#*	*2#*	*3#*	*4#*	*5#*	*6#*	*7#*	*8#*	*9#*
Ecorr(mV/SCE)	-162	57	90	89	105	-37	53	-59	196	110	168
Jcorr (nA.cm^{-2})	15.4	285	201	165	328	12.0	293	0.660	32.6	81.5	0.790
βc (x10^{-2} V/decade)	3.4	1.8	0.40	0.40	0.30	1.9	2.3	1.6	2.8	2.7	1.0
βa (x10^{-2} V/decade)	7.3	6.7	5.0	3.6	5.7	3.0	4.8	14	5.5	5.2	7.4
Rp (KΩ.cm^{-2})	657	22	9	11	4	426	24	9725	251	95	4823
Epit (V/SCE)	0.41	0.53	0.38	0.53	0.34	0.54	0.61	0.95	0.72	0.72	0.72

Porosity	-	1.6E-2	7.5E-4	8.8E-6	3.4E-3	1.1E-4	9.7E-4	1.3E-2	9.3E-7	4.5E-5	5.0E-6

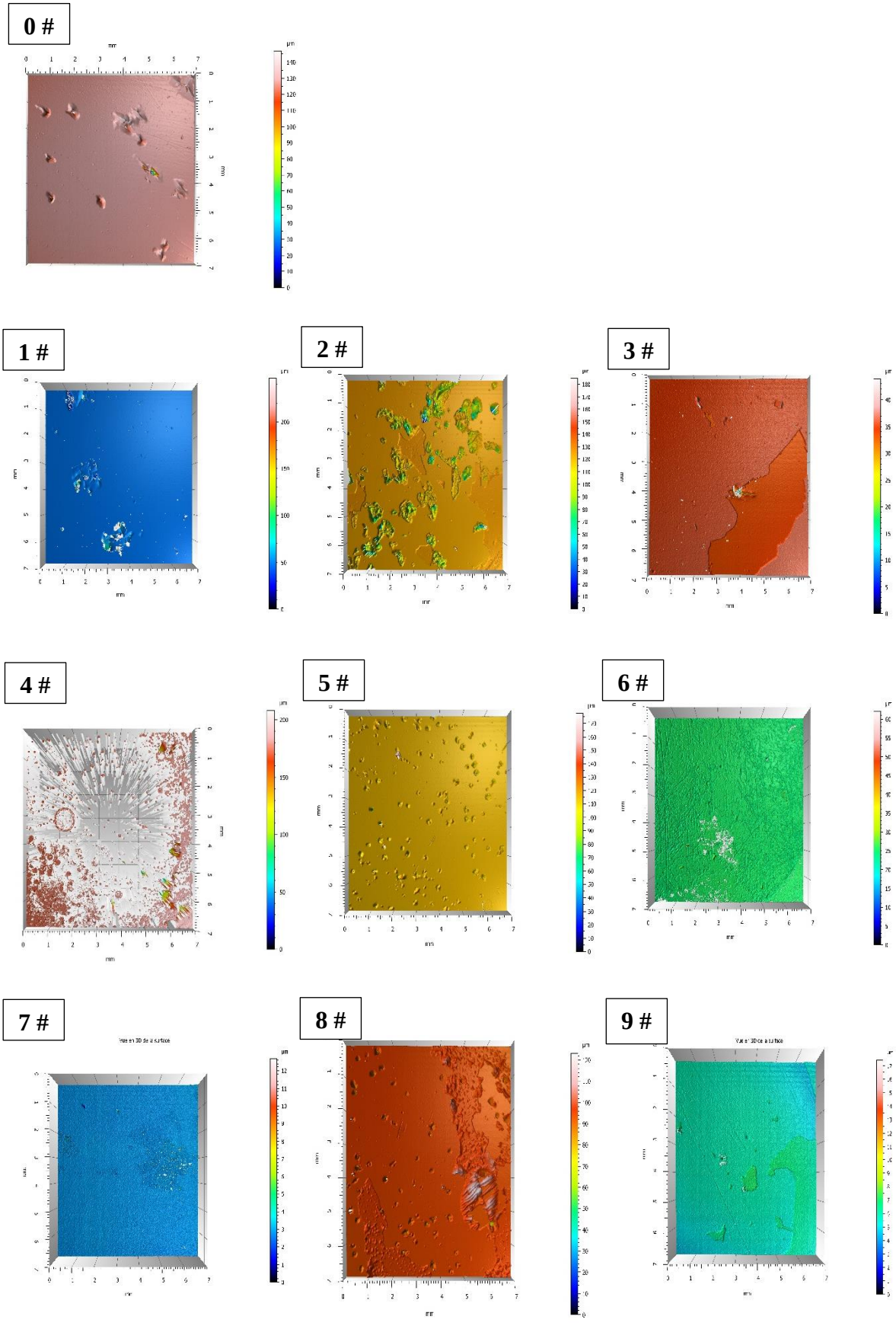

Figure 9. Surface images of the samples after corrosion tests.

4. Conclusion

In summary, different duplex coatings were deposited using the hybrid process via overlapping magnetron sputtering and atomic layer deposition thin films. The Al_2O_3, ZnO and Al_2O_3-ZnO nanolaminates were inserted within CrN coatings in different architectures: S/ALD/PVD, S/PVD/ALD and S/PVD/ALD/PVD. It consists of a comparative study for the novel approach of PVD+ALD hybrid combination. The morphology results indicates that the chromium nitride layers deposited on the three different types of ALD layers conserve their pyramidal structures and the ALD layers did not provoke any change in the growth type. Voids between S/PVD/ALD/PVD coating's particles are less pronounced compared to the S/ALD/PVD architectures. The AFM characterization attributes to the conclusion that the ALD layer insertion, whatever the architecture is, smooths the surface and therefore decreases the roughness values. XRD microstructure analysis indicates that the insertion of the ALD at any position did not provoke any phase transformation of the CrN matrix and could result in enhancing the phase stabilization of CrN. Mechanical nanoindentation tests of all the samples approved the increasing in the hardness and young's modulus of all duplex coatings compared to the as deposited CrN. This increase in hardness is due to the grain size refinement via the Hall-Petch relation. The duplex coatings presents different wettability behavior. The S/ALD/PVD coatings exhibits a hydrophilic character while The S/PVD/ALD coatings are hydrophobic. The S/PVD/ALD/PVD coatings exhibit a change in the wettability compared to CrN. The electrochemical tests were applied on the coatings to study their corrosion behavior. The insertion of an ALD layer between the substrate and the CrN layer (S/ALD/PVD architecture) slightly shifts the CrN corrosion potential to higher values whatever the inserted ALD layer type is. The S/PVD/ALD architecture coatings exhibit a decrease in the corrosion potential which could be attributed to the failure mechanism of corrosion protection of these ALD layers. The ALD is in such a position which enhances the direct interaction with the NaCl environments. These could facilitate the Cl^- ions attack to the ALD layer and accelerates its dissolution. Coatings having the S/PVD/ALD/PVD architectures present the lower porosities, which means that the insertion of the ALD as a sealing layer is more efficient in decreasing the porosities than ALD in other structures. The CrN/Al_2O_3/CrN and the CrN/$[Al_2O_3\text{-}ZnO]_n$/CrN coatings show the ability to re-passivate in the reverse scans which means that these two coatings present higher protection against pitting corrosion. We can conclude that the S/PVD/ALD/PVD architecture is the most efficient architecture to provide an improvement in corrosion resistance. The CrN/[Al_2O_3-

$ZnO]_n$/CrN coating presents the best corrosion protection performance with the lowest I_{corr} ~ 7.9 x 10^{-10} A/cm^2 lower two order of magnitude than I_{corr} of the substrate ~1.5 x 10^{-8} A/cm^2. More future studies would be helpful in the investigation and the comprehension of the ALD nanolaminates corrosion mechanism in the S/PVD/ALD/PVD coatings.

References

[1] B. Mojarad Shafiee, R. Torkaman, M. Mahmoudi, R. Emadi, M. Derakhshan, E. Karamian, F. Tavangarian, Surface Modification of 316L SS Implants by Applying Bioglass/Gelatin/Polycaprolactone Composite Coatings for Biomedical Applications, *Coatings*, vol. 10, p. 1220, 2020, https://doi.org/10.3390/coatings10121220.

[2] G. Sander, V. Cruz, N. Bhat, N. Birbilis, On the in-situ characterisation of metastable pitting using 316L stainless steel as a case study, *Corros. Sci.*, vol. 177, p. 109004, 2020, https://doi.org/10.1016/j.corsci.2020.109004.

[3] J.-Z. Kong, L. Yin, Y. Xuan, A.-D. Li, Q.-Z. Wang, F. Zhou, Atomic Layer-Deposited Al2O3 Interlayer for Improved Tribological and Anti-corrosion Properties of TiN Hard Coating on 316L Stainless Steel, *J. Mater. Eng. Perform.*, vol. 28, pp. 7058–7067, 2019, https://doi.org/10.1007/s11665-019-04427-y.

[4] M. Staszuk, D. Pakuła, G. Chladek, M. Pawlyta, M. Pancielejko, P. Czaja, Investigation of the structure and properties of PVD coatings and ALD + PVD hybrid coatings deposited on sialon tool ceramics, *Vacuum*, vol. 154, pp. 272–284, 2018, https://doi.org/10.1016/j.vacuum.2018.04.032.

[5] P. Panjan, A. Drnovšek, P. Gselman, M. Čekada, M. Panjan, Review of Growth Defects in Thin Films Prepared by PVD Techniques, *Coatings*, vol. 10, p. 447, 2020, https://doi.org/10.3390/coatings10050447.

[6] A. Ruden, E. Restrepo-Parra, A. U. Paladines, F. Sequeda, Corrosion resistance of CrN thin films produced by dc magnetron sputtering, *Appl. Surf. Sci.*, vol. 270, pp. 150–156, 2013, http://dx.doi.org/10.1016/j.apsusc.2012.12.148.

[7] L. Shan, Y. Wang, J. Li, J. Chen, Effect of N_2 flow rate on microstructure and mechanical

properties of PVD CrN_x coatings for tribological application in seawater, *Surf. Coatings Technol.*, vol. 242, pp. 74–82, 2014, http://dx.doi.org/10.1016/j.surfcoat.2014.01.021.

[8] Z. Qi, Z. Wu, D. Zhang, B. Wei, J. Wang, Z. Wang, Effect of sputtering power on the chemical composition, microstructure and mechanical properties of CrN_x hard coatings deposited by reactive magnetron sputtering, *Vacuum*, vol. 145, pp. 136–143, 2017, https://doi.org/10.1016/j.vacuum.2017.08.036.

[9] H. Li, C. Zhang, C. Liu, M. Huang, Improvement in corrosion resistance of CrN coatings, *Surf. Coatings Technol.*, vol. 365, pp. 158–163, 2019, https://doi.org/10.1016/j.surfcoat.2018.07.018.

[10] P. H. Mayrhofer, C. Mitterer, L. Hultman, H. Clemens, Microstructural design of hard coatings, *Prog. Mater. Sci.*, vol. 51, pp. 1032–1114, 2006, https://doi.org/10.1016/j.pmatsci.2006.02.002%0A.

[11] Z. Wan, T. F. Zhang, H.-B.-R. Lee, J. H. Yang, W. C. Choi, B. Han, K. H. Kim, S.-H. Kwon, Improved Corrosion Resistance and Mechanical Properties of CrN Hard Coatings with an Atomic Layer Deposited Al_2O_3 Interlayer, *ACS Appl. Mater. Interfaces*, vol. 7, pp. 26716–26725, 2015, https://pubs.acs.org/doi/10.1021/acsami.5b08696.

[12] A. G. Dirks, H. J. Leamy, Columnar microstructure in vapor-deposited thin films, *Thin Solid Films*, vol. 47, pp. 219–233, 1977, https://doi.org/10.1016/0040-6090(77)90037-2.

[13] S. Tan, X. Zhang, X. Wu, F. Fang, J. Jiang, Comparison of chromium nitride coatings deposited by DC and RF magnetron sputtering, *Thin Solid Films*, vol. 519, pp. 2116–2120, 2011, http://dx.doi.org/10.1016/j.tsf.2010.10.067.

[14] J. Lin, Z. L. Wu, X. H. Zhang, B. Mishra, J. J. Moore, W. D. Sproul, A comparative study of CrN_x coatings Synthesized by dc and pulsed dc magnetron sputtering, *Thin Solid Films*, vol. 517, pp. 1887–1894, 2009, https://doi.org/10.1016/j.tsf.2008.09.093.

[15] J. Lin, N. Zhang, W. D. Sproul, J. J. Moore, A comparison of the oxidation behavior of CrN films deposited using continuous dc, pulsed dc and modulated pulsed power

magnetron sputtering, *Surf. Coatings Technol.*, vol. 206, pp. 3283–3290, 2012, http://dx.doi.org/10.1016/j.surfcoat.2012.01.033.

[16] W. Dai, Q. Wang, K.-H. Kim, S.-H. Kwon, Al_2O_3/CrAlSiN multilayer coating deposited using hybrid magnetron sputtering and atomic layer deposition, *Ceram. Int.*, vol. 45, pp. 11335–11341, 2019, https://doi.org/10.1016/j.ceramint.2019.02.211.

[17] J. Kong, C. Li, X. Sun, Y. Xuan, H. Zhai, A. Li, Q. Wang, F. Zhou, Improved tribological properties and corrosion protection of CrN coating by ultrathin composite oxide interlayer, *Appl. Surf. Sci.*, vol. 541, p. 148606, 2021, https://doi.org/10.1016/j.apsusc.2020.148606.

[18] Z. Wan, T. F. Zhang, J. C. Ding, C.-M. Kim, S.-W. Park, Y. Yang, K.-H. Kim, S.-H. Kwon, Enhanced Corrosion Resistance of PVD-CrN Coatings by ALD Sealing Layers, *Nanoscale Res. Lett.*, vol. 12, p. 248, 2017, https://doi.org/10.1186/s11671-017-2020-1.

[19] J.-Z. Kong, P. Xu, Y.-Q. Cao, A.-D. Li, Q.-Z. Wang, F. Zhou, Improved corrosion protection of CrN hard coating on steel sealed with TiO_xN_y-TiN composite layers, *Surf. Coatings Technol.*, vol. 381, p. 125108, 2020, https://doi.org/10.1016/j.surfcoat.2019.125108.

[20] C. X. Shan, X. Hou, K.-L. Choy, P. Choquet, Improvement in corrosion resistance of CrN coated stainless steel by conformal TiO_2 deposition, *Surf. Coatings Technol.*, vol. 202, pp. 2147–2151, 2008, https://doi.org/10.1016/j.surfcoat.2007.08.078.

[21] J. Leppäniemi, P. Sippola, M. Broas, J. Aromaa, H. Lipsanen, J. Koskinen, Corrosion protection of steel with multilayer coatings: Improving the sealing properties of physical vapor deposition CrN coatings with Al_2O_3/TiO_2 atomic layer deposition nanolaminates, *Thin Solid Films*, vol. 627, pp. 59–68, 2017, https://doi.org/10.1016/j.tsf.2017.02.050.

[22] E. Härkönen, I. Kolev, B. Díaz, J. Światowska, V. Maurice, A. Seyeux, P. Marcus, M. Fenker, L. Toth, G. Radnoczi, M. Vehkamäki, M. Ritala, Sealing of Hard CrN and DLC Coatings with Atomic Layer Deposition, *ACS Appl. Mater. Interfaces*, vol. 6, pp. 1893–1901, 2014, https://doi.org/10.1021/am404906x.

[23] S. M. George, Atomic Layer Deposition: An Overview, *Chem. Rev.*, vol. 110, pp. 111–131, 2010, https://doi.org/10.1021/cr900056b.

[24] O. Graniel, M. Weber, S. Balme, P. Miele, M. Bechelany, Atomic layer deposition for biosensing applications, *Biosens. Bioelectron.*, vol. 122, pp. 147–159, 2018, https://doi.org/10.1016/j.bios.2018.09.038.

[25] M. Weber, A. Julbe, A. Ayral, P. Miele, M. Bechelany, Atomic Layer Deposition for Membranes: Basics, Challenges, and Opportunities, *Chem. Mater.*, vol. 30, pp. 7368–7390, 2018, https://doi.org/10.1021/acs.chemmater.8b02687.

[26] J. Leppäniemi, P. Sippola, A. Peltonen, J. J. Aromaa, H. Lipsanen, J. Koskinen, Effect of Surface Wear on Corrosion Protection of Steel by CrN Coatings Sealed with Atomic Layer Deposition, *ACS Omega*, vol. 3, pp. 1791–1800, 2018, https://doi.org/10.1021/acsomega.7b01382.

[27] L. H. Kim, K. Kim, S. Park, Y. J. Jeong, H. Kim, D. S. Chung, S. H. Kim, C. E. Park, Al_2O_3/TiO_2 Nanolaminate Thin Film Encapsulation for Organic Thin Film Transistors via Plasma-Enhanced Atomic Layer Deposition, *ACS Appl. Mater. Interfaces*, vol. 6, pp. 6731–6738, 2014, https://doi.org/10.1021/am500458d.

[28] B. Díaz, E. Härkönen, V. Maurice, J. Światowska, A. Seyeux, M. Ritala, P. Marcus, Failure mechanism of thin Al_2O_3 coatings grown by atomic layer deposition for corrosion protection of carbon steel, *Electrochim. Acta*, vol. 56, pp. 9609–9618, 2011, https://doi.org/10.1016/j.electacta.2011.07.104.

[29] E. Härkönen, B. Díaz, J. Światowska, V. Maurice, A. Seyeux, M. Vehkamäki, T. Sajavaara, M. Fenker, P. Marcus, M. Ritala, Corrosion Protection of Steel with Oxide Nanolaminates Grown by Atomic Layer Deposition, *J. Electrochem. Soc.*, vol. 158, 2011, https://iopscience.iop.org/article/10.1149/2.061111jes.

[30] Ü. Özgür, Y. I. Alivov, C. Liu, A. Teke, M. A. Reshchikov, S. Doğan, V. Avrutin, S.-J. Cho, H. Morkoç, A comprehensive review of ZnO materials and devices, *J. Appl. Phys.*, vol. 98, p. 041301, 2005, https://doi.org/10.1063/1.1992666.

[31] A. Abou Chaaya, M. Bechelany, S. Balme, P. Miele, ZnO 1D Nanostructures Designed by Combining Atomic layer deposition and Electrospinning for UV Sensor Applications, *J. Mater. Chem. A*, 2012, https://doi.org/10.1039/C4TA05239K.

[32] A. Abou Chaaya, R. Viter, M. Bechelany, Z. Alute, D. Erts, A. Zalesskaya, K. Kovalevskis, V. Rouessac, V. Smyntyna, P. Miele, Evolution of microstructure and related optical properties of ZnO grown by atomic layer deposition, *Beilstein J. Nanotechnol.*, vol. 4, pp. 690–698, 2013, https://doi.org/10.3762/bjnano.4.78.

[33] Z. B. Zhao, Z. U. Rek, S. M. Yalisove, J. C. Bilello, Nanostructured chromium nitride films with a valley of residual stress, *Thin Solid Films*, vol. 472, pp. 96–104, 2005, https://doi.org/10.1016/j.tsf.2004.06.116.

[34] J. Elias, M. Bechelany, I. Utke, R. Erni, D. Hosseini, J. Michler, L. Philippe, Urchin-inspired zinc oxide as building blocks for nanostructured solar cells, *Nano Energy*, vol. 1, pp. 696–705, 2012, http://dx.doi.org/10.1016/j.nanoen.2012.07.002.

[35] J. S. Daubert, G. T. Hill, H. N. Gotsch, A. P. Gremaud, J. S. Ovental, P. S. Williams, C. J. Oldham, G. N. Parsons, Corrosion Protection of Copper Using Al_2O_3, TiO_2, ZnO, HfO_2, and ZrO_2 Atomic Layer Deposition, *ACS Appl. Mater. Interfaces*, vol. 9, pp. 4192–4201, 2017, https://doi.org/10.1021/acsami.6b13571.

[36] A. Woźniak, W. Walke, A. Jakóbik-Kolon, B. Ziębowicz, Z. Brytan, M. Adamiak, The Influence of ZnO Oxide Layer on the Physicochemical Behavior of Ti6Al4V Titanium Alloy, *Materials (Basel).*, vol. 14, p. 230, 2021, https://doi.org/10.3390/ma14010230.

[37] M. Staszuk, D. Pakuła, Ł. Reimann, M. Król, M. Basiaga, D. Mysłek, A. Kříž, Structure and Properties of ZnO Coatings Obtained by Atomic Layer Deposition (ALD) Method on a Cr-Ni-Mo Steel Substrate Type, *Materials (Basel).*, vol. 13, p. 4223, 2020, https://doi.org/10.3390/ma13194223.

[38] A. Abou Chaaya, R. Viter, I. Baleviciute, M. Bechelany, A. Ramanavicius, Z. Gertnere, D. Erts, V. Smyntyna, P. Miele, Tuning optical properties of Al_2O_3/ZnO nanolaminates synthesized by atomic layer deposition, *J. Phys. Chem. C*, vol. 118, pp. 3811–3819, 2014, https://doi.org/10.1021/jp411970w.

[39] C. F. Herrmann, F. W. DelRio, S. M. George, V. M. Bright, Properties of atomic-layer-deposited Al_2O_3/ZnO dielectric films grown at low temperature for RF MEMS, *Micromach. Microfabr. Process Technol. X*, 2005, https://doi.org/10.1117/12.589322.

[40] R. Raghavan, M. Bechelany, M. Parlinska, D. Frey, W. M. Mook, A. Beyer, J. Michler, I. Utke, Nanocrystalline-to-amorphous transition in nanolaminates grown by low temperature atomic layer deposition and related mechanical properties Nanocrystalline-to-amorphous transition in nanolaminates grown by low temperature atomic layer deposition and relat, *Appl. Phys. Lett.*, vol. 100, p. 191912, 2012, http://dx.doi.org/10.1063/1.4711767.

[41] D. Osorio, J. Lopez, H. Tiznado, M. H. Farias, M. A. Hernandez-Landaverde, M. Ramirez-Cardona, J. M. Yañez-Limon, J. O. Gutierrez, J. C. Caicedo, G. Zambrano, Structure and Surface Morphology Effect on the Cytotoxicity of [Al_2O_3/ZnO]n/316L SS Nanolaminates Growth by Atomic Layer Deposition (ALD), *Crystals*, vol. 10, p. 620, 2020, https://doi.org/10.3390/cryst10070620.

[42] D. Wang, M. Hu, D. Jiang, Y. Fu, Q. Wang, J. Yang, J. Sun, L. Weng, The improved corrosion resistance of sputtered CrN thin films with Cr-ion bombardment layer by layer, *Vacuum*, vol. 143, pp. 329–335, 2017, http://dx.doi.org/10.1016/j.vacuum.2017.06.040.

[43] J. A. Thornton, High Rate Thick Film growth, *Ann. Rev. Mater. Sci*, vol. 7, pp. 239–260, 1977.

[44] G. G. Fuentes, R. Rodriguez, J. C. Avelar-Batista, J. Housden, F. Montalá, L. J. Carreras, A. B. Cristóbal, J. J. Damborenea, T. J. Tate, Recent advances in the chromium nitride PVD process for forming and machining surface protection, *J. Mater. Process. Technol.*, vol. 167, pp. 415–421, 2005, https://doi.org/10.1016/j.jmatprotec.2005.06.011.

[45] C. Gautier, J. Machet, Study of the growth mechanisms of chromium nitride films deposited by vacuum ARC evaporation, *Thin Solid Films*, vol. 295, pp. 43–52, 1997, https://doi.org/10.1016/S0040-6090(96)09164-X.

[46] J.-W. Lee, S.-K. Tien, Y.-C. Kuo, The effects of pulse frequency and substrate bias to the mechanical properties of CrN coatings deposited by pulsed DC magnetron sputtering,

Thin Solid Films, vol. 494, pp. 161–167, 2006, https://doi.org/10.1016/j.tsf.2005.07.190.

[47] M. Pakala, R. Y. Lin, Reactive sputter deposition of chromium nitride coatings on steel, *Surf. Coatings Technol.*, vol. 81, pp. 233–239, 1996, https://doi.org/10.1016/0257-8972(95)02488-3.

[48] A. Zairi, Elaboration et Caractérisation de revêtements à base de nitrure de chrome par pulvérisation cathodique magnétron en condition réactive : propriétés mécaniques et tribologiques., Ecole nationale supérieure d'arts et métiers - ENSAM 2013 Français. NNT : 2013ENAM0052. pastel-00996656.

Acknowledgments

The authors would like to thank Dr. Elia Zgheib for his help in SEM investigation.

The authors would like to thank the European Union (Fond Européen de Développement Régional) and the Doctoral School in Sciences and Technology at the Lebanese University (Réseau UT/INSA-UL) for their financial support.